2-9063

ISQ82-00064

Final Report

by

The Research and Productivity Council

rpc

RESEARCH AND PRODUCTIVITY COUNCIL

LE CONSEIL DE RECHERCHE ET DE PRODUCTIVITE

Development of an Erosivity Test for The Characterization of Coal Water Liquid Fuels

Final Report

by

The Research and Productivity Council

Work on this project was conducted under the auspices of the Canada Centre for Mineral and Energy Technology, Energy, Mines and Resources, Canada.

DSS FILE NUMBER	:	26SQ.23440-2-9063
DSS CONTRACT SERIAL NUMBER	:	1SQ82-00066
CANMET PROJECT NUMBER	:	435001
CANMET SCIENTIFIC AUTHORITY	:	Dr. G. R. Hoey

Date: August 3, 1983

This report should be cited as Contract Report No: 1SQ82-00066.

72 pp

RPC Report 96-0144/12

Authors K. G. Sedman, J. C. Thornley

This work was performed for the Physical Metallurgy Research Laboratories, CANMET, Energy, Mines and Resources, Canada under Supply and Services Canada Contract 1SQ82-00066.

Any data presented, opinions, findings, conclusions, or recommendations expressed in this report are those of the authors and do not necessarily reflect the views of CANMET.

Crown copyright of this report is reserved.

TABLE OF CONTENTS

		Page
1.0	ABSTRACT	1
2.0	INTRODUCTION	2
	2.1 Background and Objectives	2
	2.2 Previous Work	2
3.0	EQUIPMENT	4
	3.1 Piping, Storage and Pumping	4
	3.2 Nozzle and Target	5
	3.3 Coal and Slurry Production	10
	3.3.1 Coal Comminution	10
	3.3.2 Slurry Mixing	10
	3.4 Erosion Test Procedure	13
	3.5 Cycled Slurry Examination	15
4.0	RESULTS	16
	4.1 Erosion	16
	4.2 Viscosity and pH	22
	4.3 Particle Size	29
	4.4 Mineralogy	34
5.0	DISCUSSION	46
	5.1 The Erosive Peak	46
	5.2 The Cause of Peaking	47
	5.3 Significance of Peaking with Respect to Erosion Testing	48
	5.4 Relative Erosion Resistance of Four Target Materials	49
6.0	CONCLUSIONS	50
7.0	REFERENCES	52
APPENDIX	Corrosion of Metals by Coal-Water Mixtures	53

LIST OF TABLES

		Page
TABLE 1	Chemical Analysis of the Crushed Coal	11
TABLE 2	Particle Size Distributions of the Crushed Coal	12
TABLE 3	Erosion Resistance of Various Target Materials	14
TABLE 4	Solids Loading	23
TABLE 5	Sieving Results of Trial 1	31
TABLE 6	Sieving Results of Trial 2	32
TABLE 7	Sieving Results of Trial 3	33
TABLE 8	X-Ray Diffraction Examination of that Fraction Sinking in a Liquid of 2.4 S.G.	35
TABLE 9	The Shape of the Pyrite Grains	38
TABLE 10	Pyrite Particle Sizes in the Sink Fraction for Trial 1	39
TABLE 11	Pyrite Particle Sizes in the Sink Fraction for Trial 2	40
TABLE 12	Pyrite Particle Sizes in the Sink Fraction for Trial 3	41
TABLE 13	Percentage of Free Pyrite	45

APPENDIX

TABLE A1	Water Line Corrosion of Various Materials Due to Coal-Water Fuels	57
TABLE A2	Corrosion of Various Materials Placed at the Bottom of a Coal-Water Fuel Storage Tank	58

1.0 ABSTRACT

The effects of recycling a coal and water fuel through an erosion test loop on the properties of that fuel were studied. The erosion test loop was a partial simulation of a burner nozzle. The erosiveness of the coal-water fuel was observed not to be a monotonic function of recycling but was observed to rise to a peak and then drop off. Over the period of 400 cycles the viscosity of the slurry increased and the pH decreased. The coal grains were smaller and rounder at the end of the erosion trials. The same effect occurred to the pyrite grains which were also observed to become more liberated from the coal with recycling. All of these changes to the slurry and coal characteristics were measured and compared to the overall slurry erosiveness with respect to recycling. This was done in order to determine the feasibility of erosion testing using recycled coal-water fuel.

2.0 INTRODUCTION

2.1 Background and Objectives

The erosivity of liquid fuels containing powdered coal has led to erosion problems in burner nozzles, pumps, piping, and valves (1,2,3), but particularly in nozzles. Before these fuels are burnt in a particular system, there is a clear need to perform erosion tests on candidate components or materials which are to see service in plants burning, or manufacturing coal/liquid fuel mixtures (CLM). In order to be valid, this testing must be for a substantial period and there are two alternative test methods. One is to take a large quantity of fuel and pass this through the component being tested once only. The other alternative is to take a lesser quantity of fuel and to recirculate that fuel through the component many times to provide the necessary operating time. This second procedure is generally the more economical regarding fuel usage but there is a problem with it in that the fuel itself is changed by the re-cycling and one might expect it's erosiveness to change. The fuel will change, for example, as a result of the coal particles in the fuel abrading against each other and against the device being tested.

The work performed here, therefore, is to determine what changes take place in a recirculated fuel and how those changes affect the erosiveness of the fuel. Passage of coal-water slurry through a small orifice and against a target plate has been used to simulate a burner nozzle, and burner nozzles are the components at greatest risk from erosion.

2.2 Previous Work

The erosion rate of various materials has been observed to vary directly with the velocity of the CLM. Raask (4,5) found that using boiler tube steels, the amount of metal wear per unit time is proportional to $V^{3.5}$, where V is the velocity at impact. The impingement angle of the fuel to the eroding material has also been observed to

affect the erosion rate. An angle of 30° - 35° yields a maximum erosion rate in ductile materials, depending on the material being eroded (5).

Smaller size particles tend to follow flow changes more readily than do larger size particles. Thus the size distribution can drastically affect the erosion rate. The viscosity of the fluid in which these particles are suspended would determine what size of particles would not follow changes in flow and at what velocity these particles would contact the target. Thus the erosion rate would on this basis be expected to decrease with increasing viscosity of a CLM. In air, for example, Tilly (6) found that at a velocity of 104 m/s silica particles of 5μm or less essentially followed the flow line.

The abrasiveness of coal is related to the hardness and relative density of the coal itself, the degree to which the coal is naturally fractured (cleat development), and the mineral matter content. The Vicker's hardness of coal in general increases with increasing carbon content to about 37 kg/mm^2 at 80 percent carbon. Studies (7) have indicated that the highest values of hardness would be expected in the bright or highly reflective coals high in vitrinite macerals (coalified wood tissues) and low in exinite macerals (coalified resinous and waxy materials of plants) such as the ones in this study. By far, the greatest factor affecting the abrasiveness of coals is the mineral matter content which will be the main subject of this report. Of the common minerals in coal, those that have the highest hardness are quartz (820 kg/mm^2), pyrite (625 kg/mm^2), and magnetite (560 kg/mm^2).

The Technical University of Nova Scotia carried out a study of burner tip erosion with coal/liquid mixtures from which they concluded that the most important factors in controlling erosion rates of burner tips are impingement velocity and the presence of large, hard, and sharp-edged particles (8).

The TUNS work was performed with coal-oil-water fuel mixtures and from their results the TUNS investigators concluded that the erosiveness of their fuel remained unchanged for up to 15 recirculations. Conclusions regarding changes of the size and shape of the coal particles were not definite.

3.0 EQUIPMENT

3.1 Piping, Storage and Pumping

The project started on September 1, 1982 and the construction of the apparatus was completed on December 13, 1982. The apparatus for the erosion testing needed to be capable of storing, pumping, and then spraying a stream of coal water slurry onto a target metal sample. The amount of slurry required for each complete trial was 1140 litres (250 imp gal). The slurry was pumped at a constant rate of 19 l/min giving a 40 m/s jet velocity as the stream left the 3.2 mm diameter nozzle. The total time required to recirculate the 1140 litres of slurry at the required flow rate was 60 minutes. This allowed the erosion testing of several targets to be completed with slurry from any one cycle. The erosion apparatus is shown in Figure 1.

In order to know unambiguously how many cycles each coal particle has made, two 1140 litre storage tanks were installed and used initially. Hence, initially, the slurry was drained from one tank and added to the other, completing one cycle. Stirrers were mounted in the tanks in order to keep the slurry well mixed. A smaller subsidiary tank was installed so that the pump and lines could be cleaned after use. This tank was filled initially with clean water. Prior to the pump being allowed to remain off for any substantial period, water was pumped from this small tank through the pump and back to this tank. Hence, most of the slurry, which might have settled out in the pump, was removed and was prevented from causing problems.

However, during the first trial it was recognized that draining from one tank and refilling the second one resulted in non-uniformity of the slurry from the start to the completion of a single 60 minute cycle. This gave unacceptable "scatter" in erosion results (see Figure 5) and later, the use of two tanks was discontinued.* The flow arrangement which was used for Trials 2 and 3 and for all but the first 15 cycles of Trial 1 is shown in Figure 2.

*This and several other procedural changes, from the procedure written in the contract, were made with the consent of the Scientific Authority.

A Moyno progressive cavity pump (Model 3L6) and matching Sterling variable speed drive motor (Model 184 TC-E72-23) were used to pump the coal water slurry. The variable drive motor allowed the flow rate to be continuously adjusted to 19 l/min despite changes in the slurry viscosity with increasing recycling.

3.2 Nozzle and Target

The nozzle was manufactured around a standard polished tungsten carbide drawing die that already contained a 3.2 mm (0.125 inch) diameter hole. A section through a nozzle is shown in Figure 3. This design of the nozzle allows the insert to be easily inspected or changed. The sample specimens are mounted on stands that were at an angle of 45° to the impinging stream of slurry. The impingement angle of 45° was chosen in order to allow comparison of the work here with the earlier TUNS studies where 45° had also been used as a target plate angle (9). The distance from the nozzle opening to the sample plate was 20 mm. The spray chamber is shown in Figure 4. Six sample holders were mounted on a carousel which could be rotated. Thus six sample plates could be loaded, and, without stopping the pump all six could be sequentially exposed to the action of the slurry. The carousel can be seen in Figure 4.

Four target materials were used. Pure aluminum (99.99% Al) was used as a target plate in all three campaigns. In addition, hardened Grade 416 stainless steel was employed in the first and second campaigns while tungsten carbide targets replaced the stainless steel in the third campaign. Reynolds Alumina was used as a target material twice in the third campaign.*

* This alumina was of 99.7 percent theoretical density and was supplied by Dr. S. Whiteway of the Atlantic Research Laboratory of NRC.

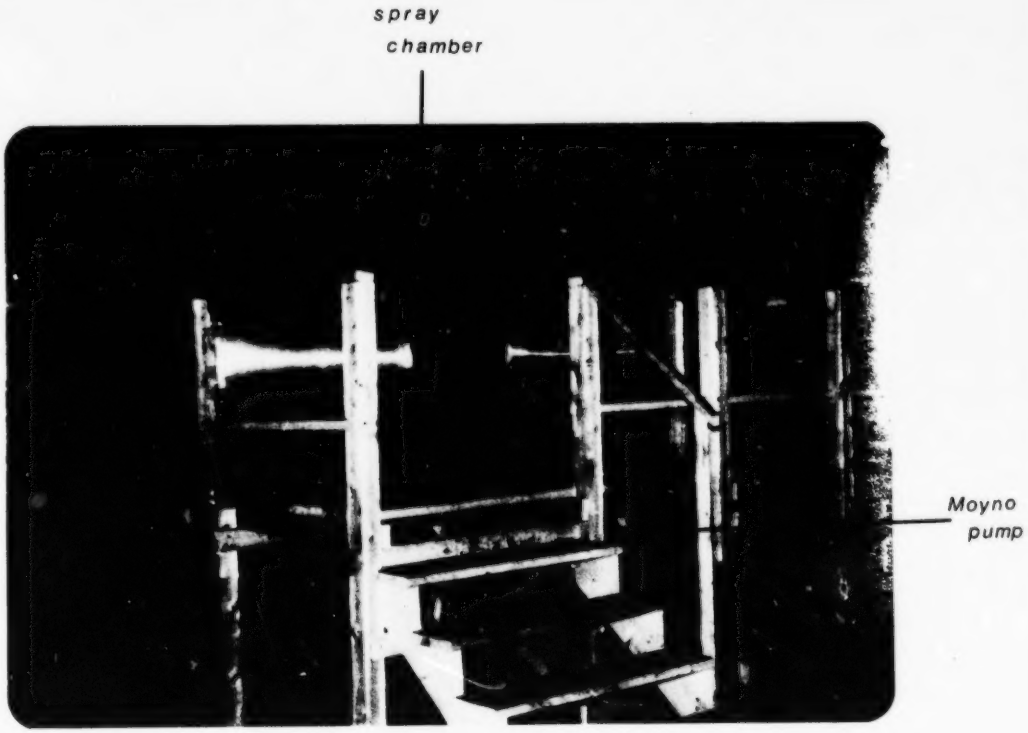

Figure 1

The erosion test apparatus containing: two storage tanks, one purge tank, the Moyno pump, the spray chamber, and two stirrers. After the experimental procedure was changed due to irregularities in the slurry properties, only one of the storage tanks was used. A second stirrer was added to this tank at this time to facilitate better slurry mixing.

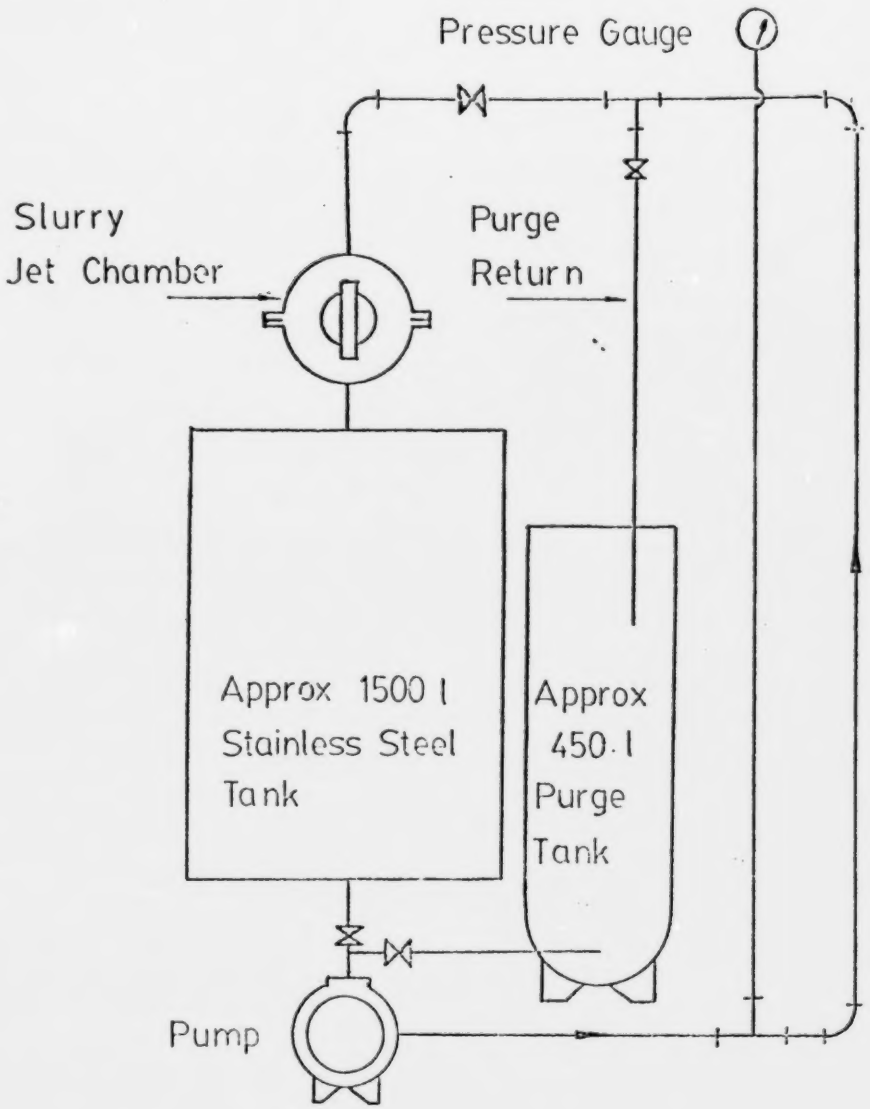

Figure 2

Piping arrangement adopted for all but the first fifteen cycles of Trial 1. The slurry is simply pumped from a storage tank, passed through a nozzle and impinges onto the target plate before returning to that storage tank.

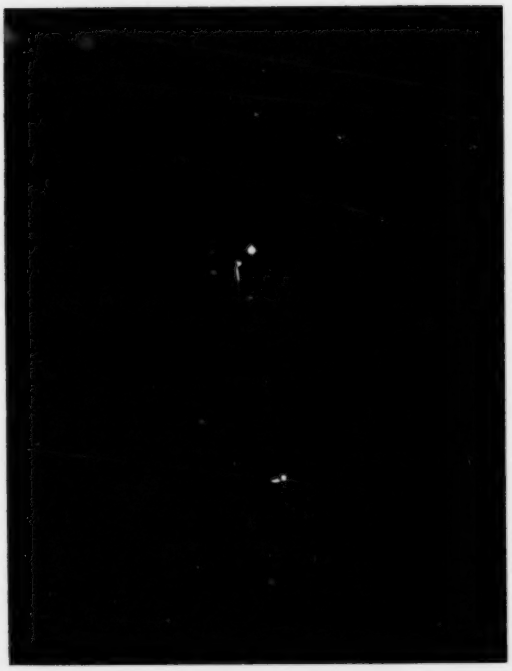

Figure 3

A section through a polished tungsten carbide nozzle of 3.2 mm (1/8 inch) diameter. The nozzle was purchased as a wire drawing die and required only minor modifications to make it suitable for the purposes here.

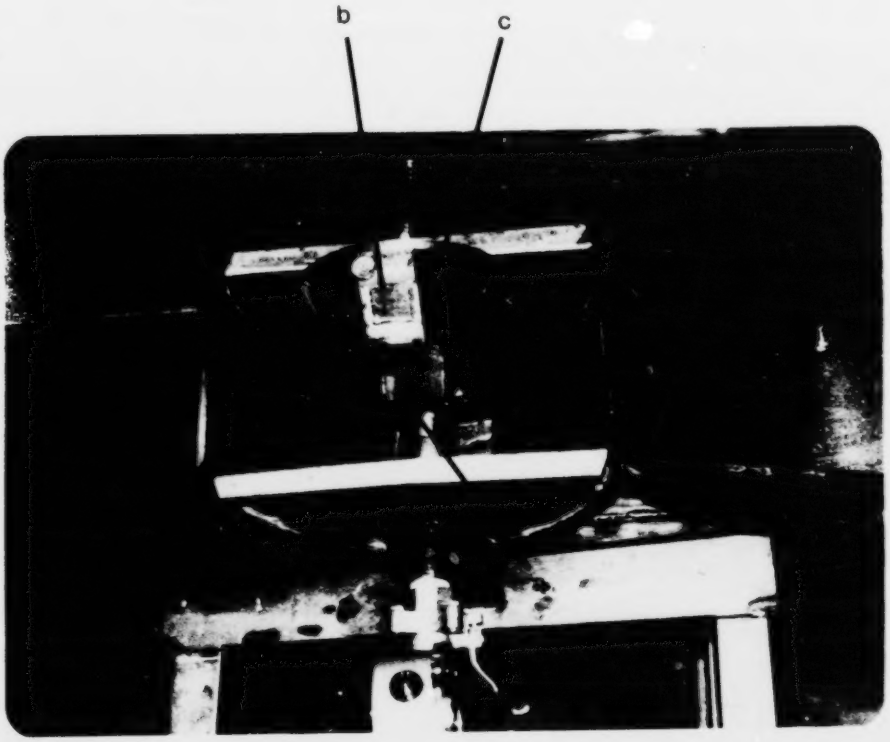

Figure 4

Spray Chamber

a) nozzle

b) sample stands

c) carousel

3.3 Coal and Slurry Production

3.3.1 Coal Comminution

Washed thermal coal was purchased from Devco for use in the project. The coal was crushed in a ball mill at RPC to 75 percent less than 200 mesh (75 μm) with a top size of 231 μm which was achieved by screening at 64 mesh. The coal was crushed to this specific particle size distribution since it is a common distribution of pulverized fuel for utility boilers. Screening was necessary in order to remove particles which otherwise caused nozzle blockage.

A detailed analysis of the crushed coal, which was used in each trial, was performed after the coal was blended into a slurry to insure complete mixing. The results of the proximate analysis, ash analysis, calorific value, and sulphur content are listed in Table 1. The particle size analysis of the mixed coal for all three trials is displayed in Table 2.

The samples for the coal analysis were obtained from the mixed 50 percent coal and water (by weight) slurries in order to ensure complete mixing. The samples were filtered and dried at 40°C for four hours prior to being analysed.

3.3.2 Slurry Mixing

A 50-50 by weight coal to water slurry was mixed using the crushed thermal coal. Experimental mixing of the coal to water slurry concluded that a wetting agent was required so the dispersant A-23 was obtained from Diamond Shamrock. A-23 is an ammonium-based product that was added to the level of 0.20 percent of the coal's weight. At this level of addition of A-23 dispersent the coal was easily wetted and mixed to the required loading. No other additives were used either on initial mixing or during the tests.

TABLE 1

CHEMICAL ANALYSIS OF THE CRUSHED COAL

Trial No.	Proximate Analysis (wt%)				Ash Analysis (wt%)							Sulphur (%)	Gross Calorific Value	
	Moisture	Ash	Volatiles	Fixed Carbon	SiO_2	Al_2O_3	Fe_2O_3	CaO	MgO	Na_2O	K_2O		J/g	BTU/lb
1	1.07	10.79	34.27	53.9	33.80	25.65	38.60	1.15	0.78	0.46	1.26	3.54	31092	13367
2	0.73	9.26	34.00	56.01	34.76	24.92	38.32	1.10	0.81	0.46	1.22	3.61	31196	13412
3	1.10	10.22	32.39	56.29	33.21	22.54	38.78	1.20	0.80	0.28	1.44	3.07	31280	13448

The chemical analysis indicates that the coal used for erosion testing in this paper was a high volatile butiminous coal.

TABLE 2

PARTICLE SIZE DISTRIBUTIONS OF THE CRUSHED COAL

Particle Size μm	Mesh Size	Cumulative Weight (%) Greater Than The Listed Particle Size		
		Trial 1	Trial 2	Trial 3
149	100	6.7	5.9	6.93
105	140	15.6	10.0	14.95
90	170	18.1	16.7	17.82
75	200	23.9	20.9	21.98
63	235	25.7	23.0	23.84
53	270	32.9	29.1	32.24
44	325	36.4	31.5	33.61

The actual coal particle size distributions varied from between 76.1 - 79.1 percent less than 200 mesh (75 μm).

3.4 Erosion Test Procedure

A variety of target materials with a wide range of hardnesses were utilized during the erosion trials, as mentioned in Section 2.2, in order to measure any significant differences in their erosion properties. These materials were 99.99 percent pure aluminum, hardened Grade 416 stainless steel, cemented tungsten carbide, and ARL's Reynolds Alumina (density >99.7 percent of theoretical). Due to the significant differences in the erosion resistance of these materials they were exposed to the coal-water slurry for different periods of time. The aluminum targets were exposed for a period of 10 minutes while the Grade 416 stainless steel and tungsten carbide targets were exposed for 20 and 30 minutes respectively. Only one alumina target was exposed and it was exposed once for one hour on one side and once again for 20 hours on the other side. The typical examples of weight losses which occurred to these materials when they were exposed to fresh coal-liquid mixture (CLM) are listed in Table 3. The accuracy to which all of the weight loss measurements were made was plus or minus 0.1 mg.

During the erosion trials the flow rate was tested at least daily and also just before an erosion test. The flow rate was determined by measuring the time required for 10 litres of slurry to be collected in a bucket as the slurry left the spray chamber. Slurry samples for slurry characterization were also taken just before a scheduled erosion test. The slurry sample was taken from the nozzle rather than from the tank. Samples were taken and erosion tests were made after the following number of previous cycles which the CLM had experienced: 0, 1, 3, 5, 10, 20, 35, 70, 100, 150, 200, 250, 300, and 400. These periods are, very approximately, equally spaced if one takes their common logarithms. Ten litres of slurry was taken as it left the nozzle. Half of this was frozen while the other half was filtered and dried. However, before filtering the water off, several measurements of the CLM properties were made. These were the CLM's viscosity, using a Brookfield viscometer, pH, and slurry solids concentration.

TABLE 3

EROSION RESISTANCE OF VARIOUS TARGET MATERIALS

Target Material	Weight Loss mg/minute	Average Vicker's Hardness
[1]Aluminum 99.99% Pure	6.1	25.1*
[2]Grade 416 Stainless Steel	1.5	525*
[3]Tungsten Carbide	7.1×10^{-2}	1782+
[3]Reynolds Alumina >99.7% of theoretical density	1.3×10^{-2}	≅2000

* Hardness measured using a 5 kg load

\+ Hardness measured using a 30 kg load

1 Erosion tested in all three trials

2 Erosion tested in Trials 1 and 2

3 Erosion tested only in Trial 3

Reynold's Alumina was clearly the most resistant material to the erosive spray of the coal-water mixture. This was in part due to its chemical inertness but, as will be concluded in a latter section, was mainly a result of its hardness.

The erosion measurements in the above tables were averaged from the experimental results of freshly prepared slurry (within the first three cycles).

3.5 Cycled Slurry Examination

The solid fraction of each sample of slurry was filtered off and dried and then examined to determine the particle size distribution, mineral abundances, and the particle shape. The particle size distribution was measured using wet screening and an image analyser, or Quantimet. In order to examine the changes in the mineral constituents, specific gravity separations were conducted at an S.G. of 2.4. This concentrated the heavy mineral fraction which was then examined separately using X-ray diffraction techniques to determine what minerals were present and their relative abundance. The concentrated mineral fraction was also examined microscopically and with the use of a Quantimet. These examinations were conducted in order to determine the mineral size, shape, degree of rounding, as well as the amount of free quartz and free pyrite.

4.0 RESULTS

4.1 Erosion

The change in erosiveness of the three lots of trial mixtures with respect to recycling is displayed in Figures 5, 6, 7, and 8. It is immediately apparent that the slurry's erosiveness was not a monotonic function of its cycling history. These curves indicate that the slurry becomes more erosive with time then reaches a maximum (or peak) value between 20 and 100 cycles whereafter the slurry becomes progressively less erosive with time. The location and magnitude of the peak erosivity of the CLM, for the various trials, was different. This indicates that the slurry's solids content, particle size distribution, and coal characteristics may directly affect the degree of erosivity and the location of these peaks. The position of the peak might also be influenced by the abrasiveness of the target plate towards the coal particles.

When the positive slope (initial part of the curve) of the erosiveness against recycling curve was first seen, it was not known whether this was a real slurry property or whether it was an artifact of the testing procedure. A particular concern was that wear in the nozzle might be causing this effect. To examine this hypothesis several nozzles were used in quick succession on a fairly old slurry (110 cycles). One of these nozzles was brand new, a second had had 40 lots of 1140 litres pumped through it, and the third and fourth were more seasoned still: they had had 170 and 400 of the 1140 litre tanks full pumped through them respectively. The weight loss in the erosion trials with the aluminum target plate did not depend in any way upon the history of the nozzle (Figure 9).

Secondly, one nozzle was left in place following one campaign and used for the succeeding one. The rise, peak, and fall in erosion was obtained in exactly the same way for the two campaigns but with the same nozzle.

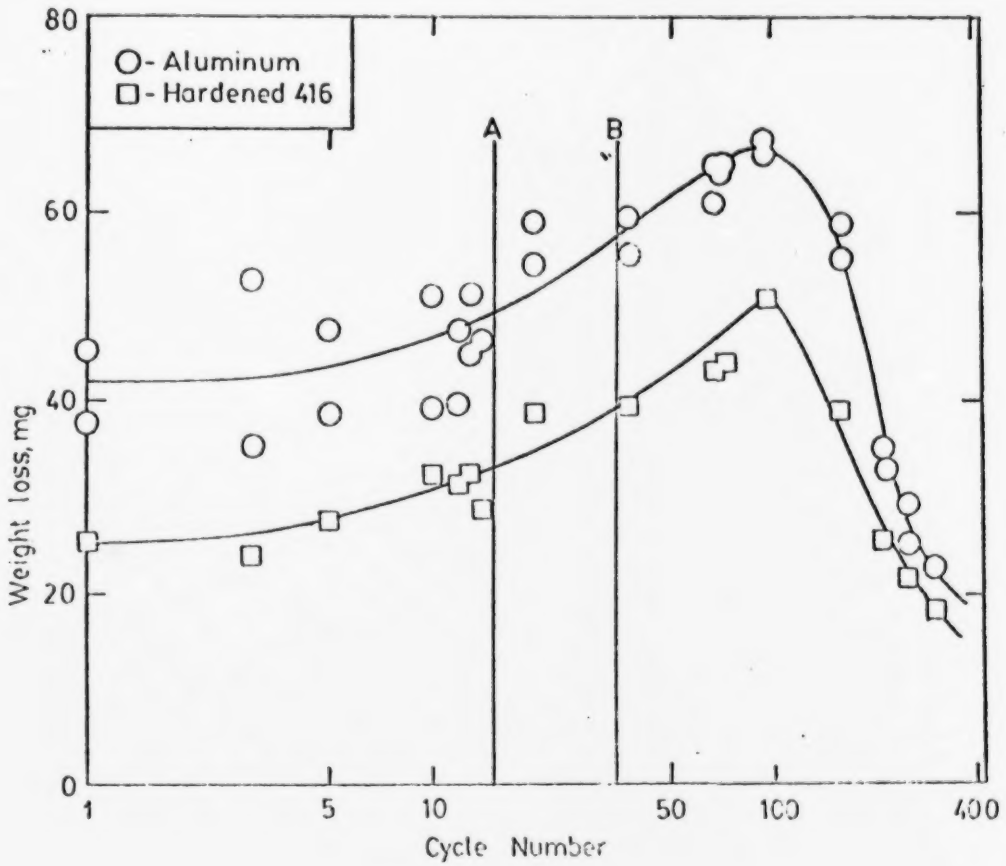

Figure 5 Erosion results from the first trial. Note here, and in Figures 6 and 7, that the weight loss during a test rises to a maximum and then falls. Note also in this Figure only, that there is serious scatter in the results from the aluminum sheet during the first fifteen to thirty cycles.

At Point A the use of two tanks was discontinued and at Point B a second stirrer was added to the single tank being used. Both of these changes reduced the scatter in the duplicate erosion tests on aluminum.

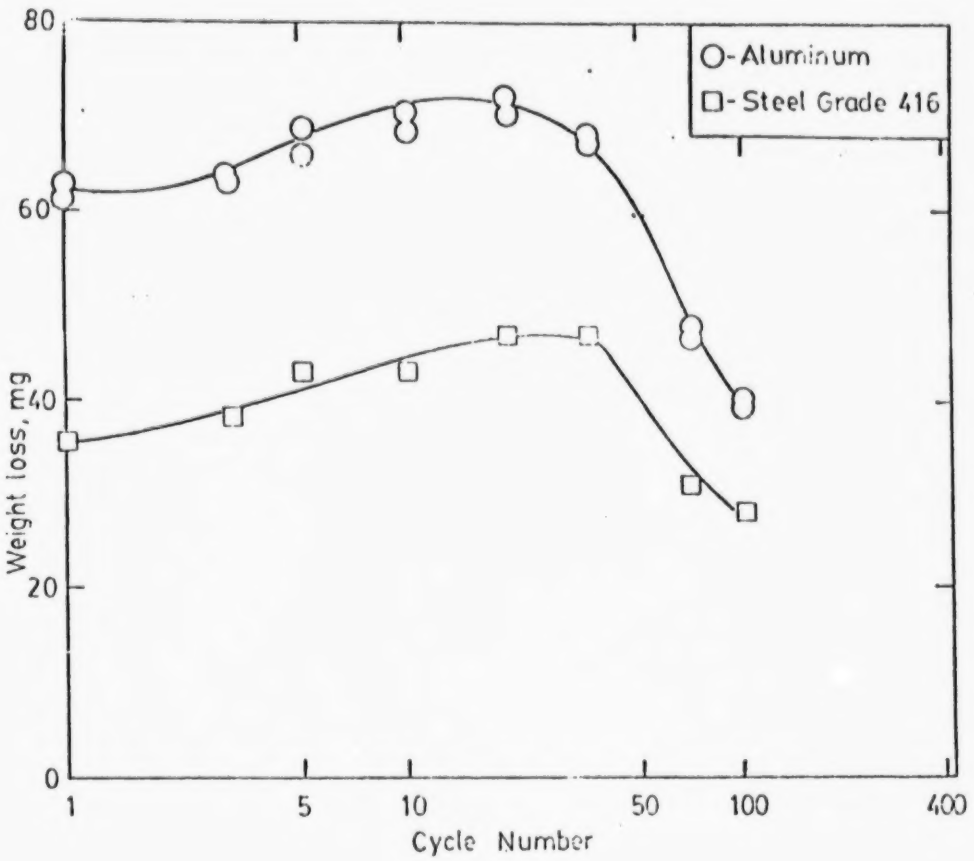

Figure 6 The pattern of rising and falling weight losses is similar here to Figure 5 except that the scatter apparent during the first trial has been eliminated. These results are from the second trial.

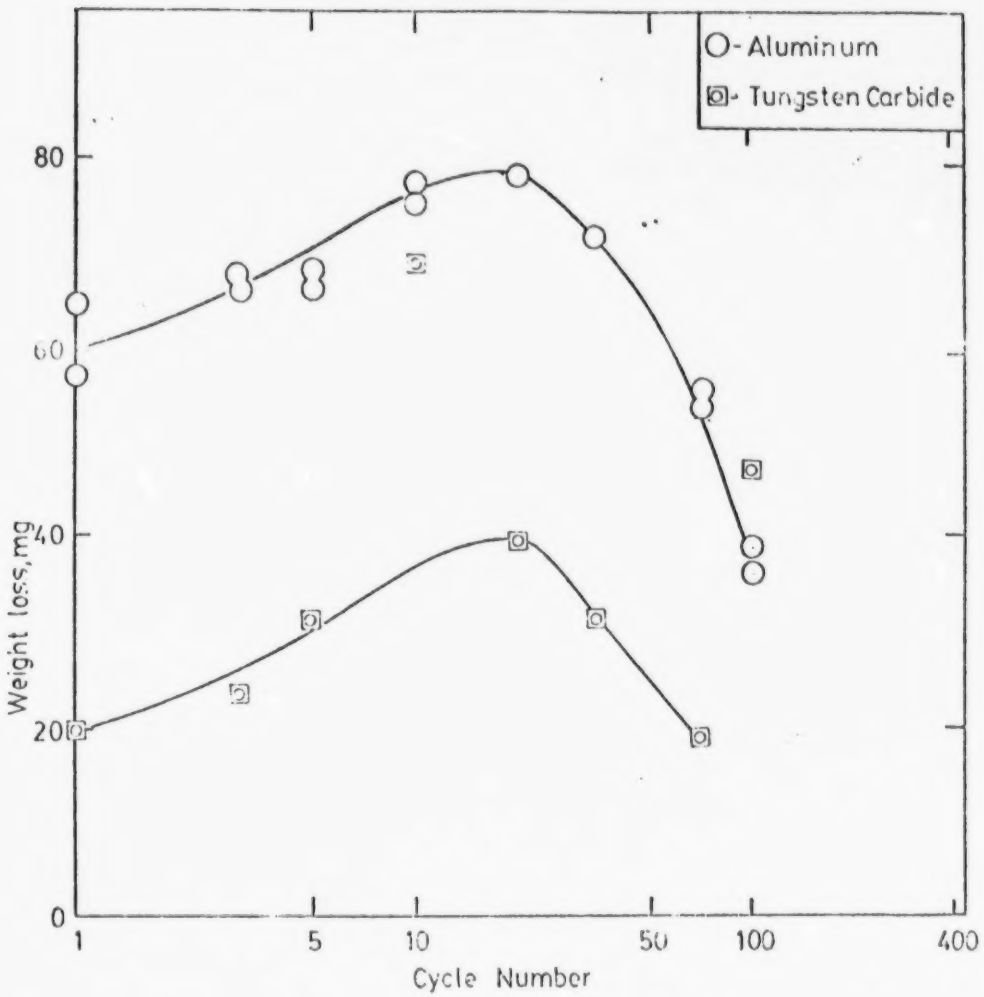

Figure 7 Again the pattern of weight loss as the slurry ages is as in Trials 1 and 2. Here, however, we have aluminum and tungsten carbide rather than aluminum and hardened type 416 stainless steel. These data are from the third trial.

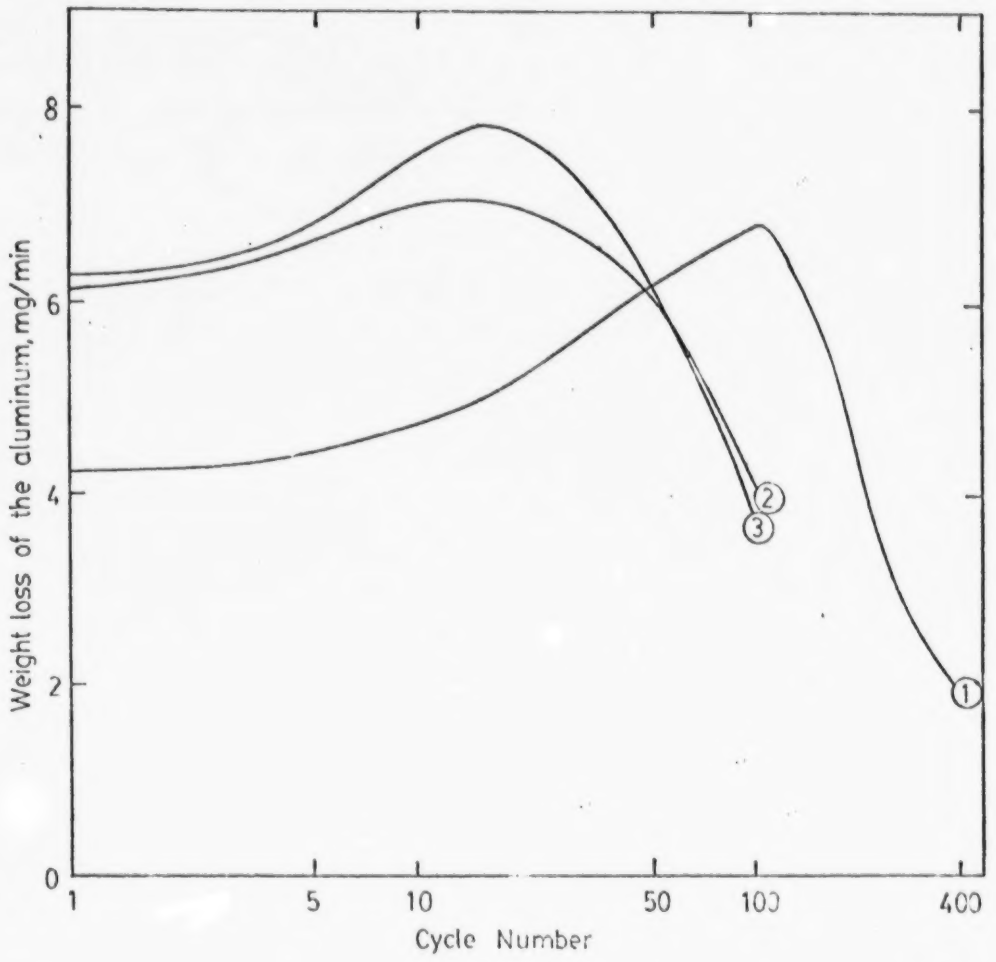

Figure 8 Combined erosion curves, for aluminum only, from all three trials expressed in weight loss per unit time. The principle difference between slurry 1 and the other two is believed to be in the particle size distribution (Table 2). The first slurry was the coarsest.

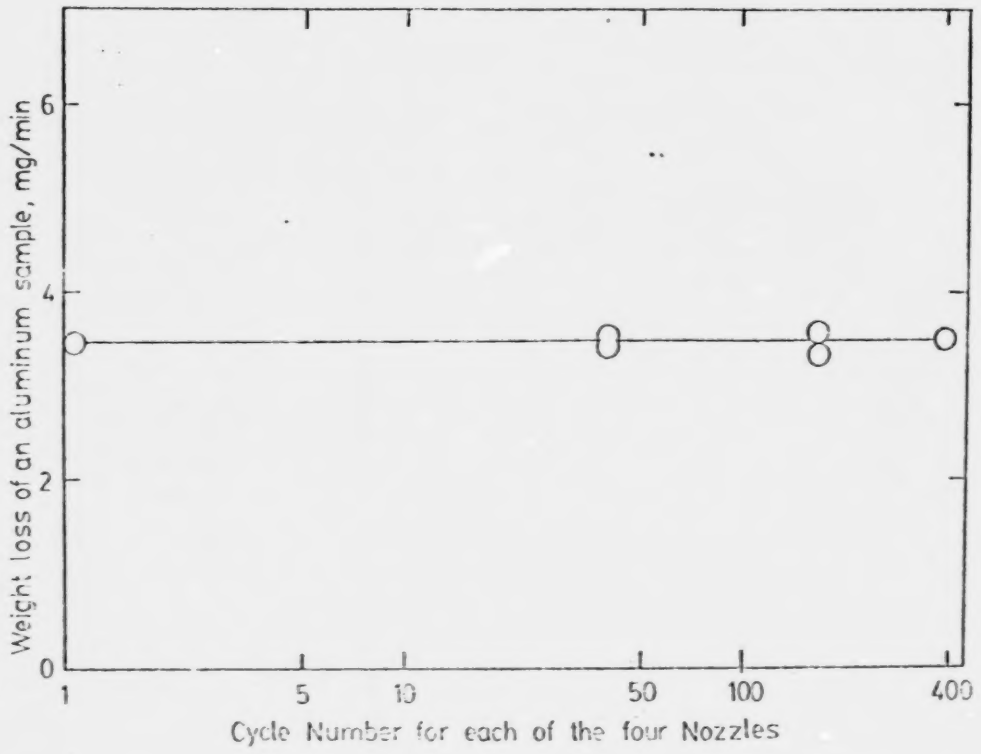

Figure 9 Four nozzles were used in quick succession and the effect of prior nozzle history upon weight loss was measured. There was found to be no effect whatever of nozzle history upon weight loss for up to 400 hours of operation with a slurry velocity of 19 m/s.

It was concluded at this stage that the peaking behaviour of the slurry's erosiveness was a real slurry property rather than an experimental artifact. Other parameters such as velocity, impingement angle, and solids loading, which would also affect the erosion weight loss, remained as near constant as could reasonably be achieved during the trials. The solids loading variations with recycling are displayed in Table 4.

The peaking behaviour observed in the aluminum erosion trials was repeated in the case of both the hardened martensitic stainless steel and when cemented tungsten carbide was erosion tested (Figure 10). The erosion experienced by each of these three materials, and of the harder alumina, is shown in Figure 11. It must be kept in mind that the variances in slurry characteristics in the three runs restricts exact comparison of the Grade 416 stainless (tested in Trial 1 and 2), tungsten carbide, and Alumina (both of which were tested in the third trial).

The Reynold's Alumina exhibited the greatest resistance to erosion as would be expected due to its high hardness and chemical inertness.

4.2 Viscosity and pH

The change in the viscosities of the recycled coal liquid mixtures is displayed graphically in Figure 12. These curves indicate that the viscosity of the recycled slurry is constant for at least five cycles after which the viscosity increases. The exact duration of the initial period of constant viscosity varies for each trial. It was approximately five cycles for Trial 2, ten cycles for Trial 3, and 100 cycles for Trial 1. Since the viscosity of a CLM fuel is known to vary with respect to the coal particle size distribution (9), the length of the period of constant viscosity is considered to be a slurry characteristic. In other words, a specific particle size distribution must be reached before the viscosity increases.

TABLE 4

SOLIDS LOADING

Number of Previous Cycles	Solids Loading (%) Trial 1	Trial 2	Trial 3
0	50	50	50
1	50	50	48
3	45	50	48
5	48	50	45
10	42	50	45
20	43	49	45
35	44	50	46
70	43	51	44
100	41	50	40
150	41	—+	—++
200	39	—	—
250	39	—	—
300	40	—	—
400	41	—	—

+ Trial 2 stopped

++ Severe dilution and loss of slurry made these numbers unrepresentative

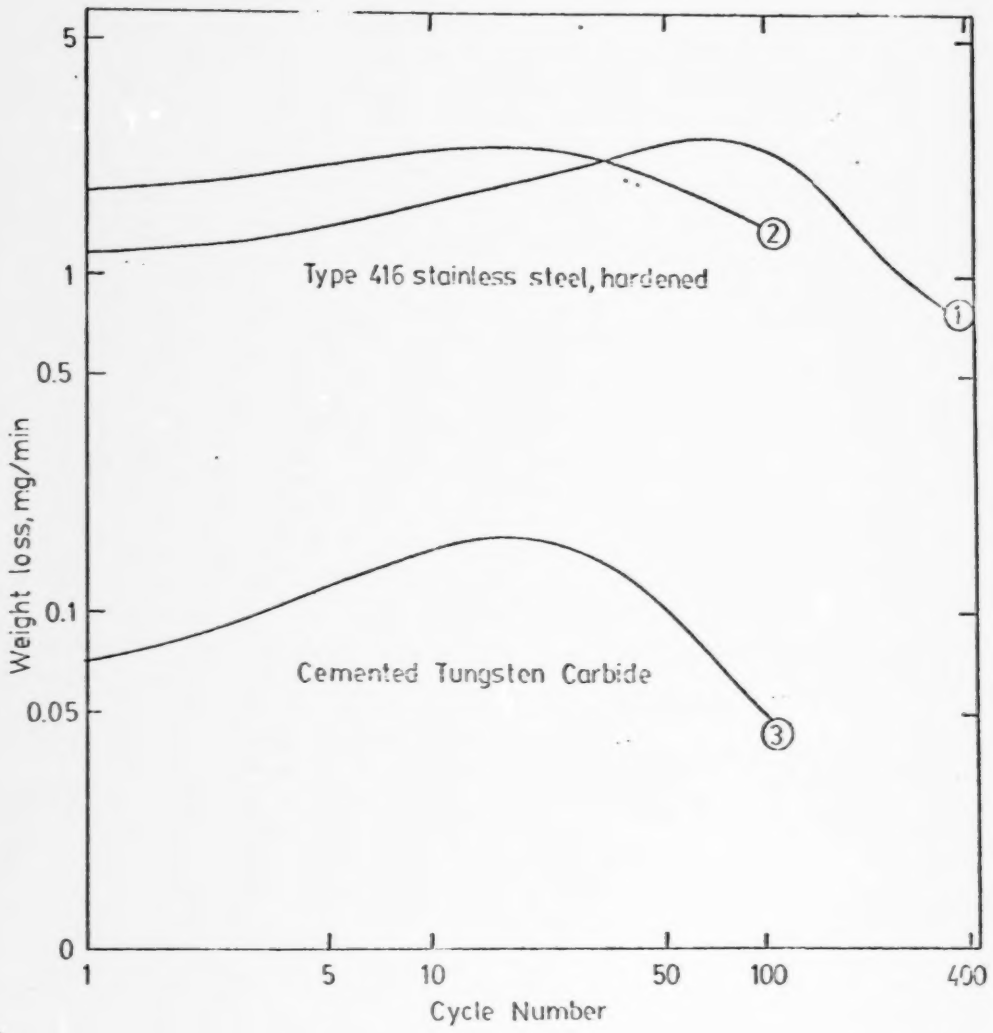

Figure 10 Weight losses of the two intermediate hardness materials followed the same pattern as did the weight losses in the aluminum trials. There was insufficient alumina available to determine the erosion recycling pattern for it.

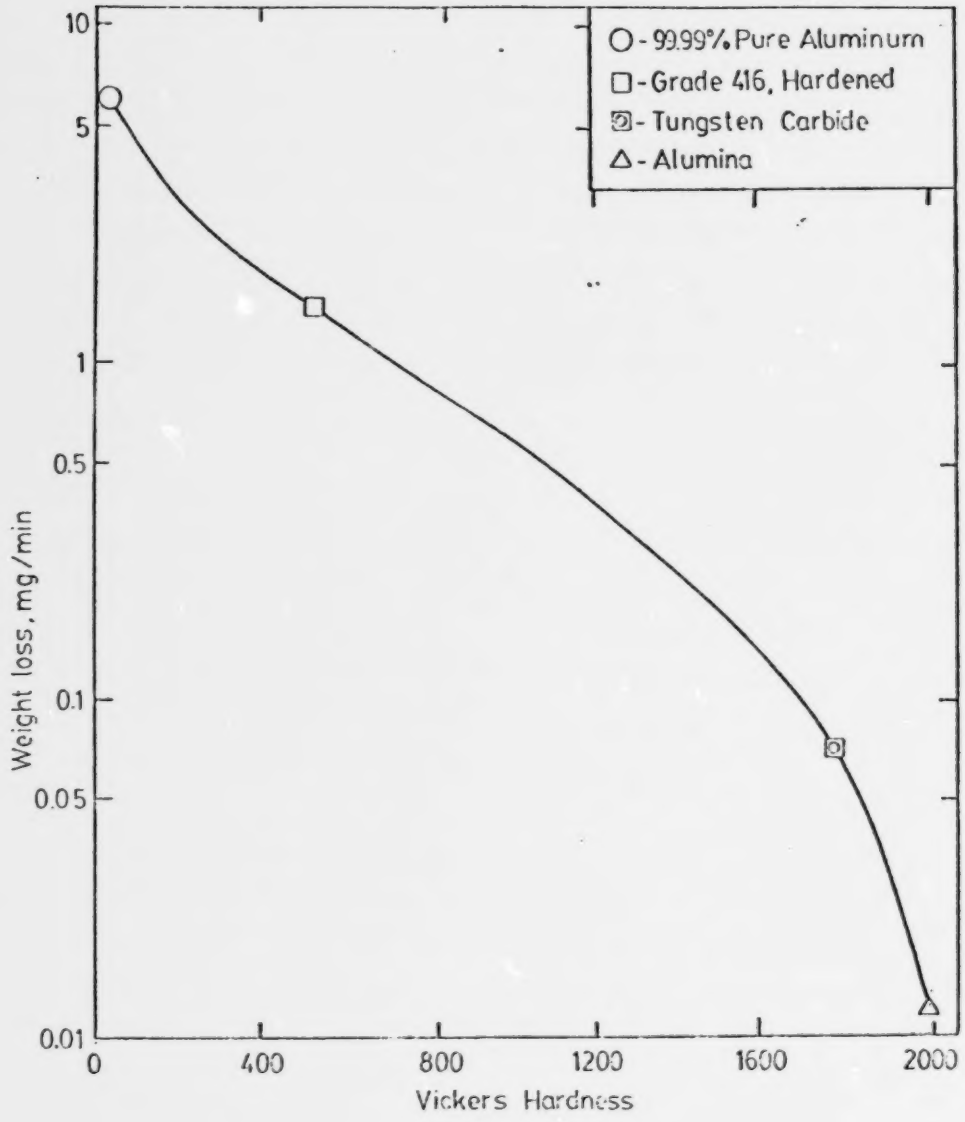

Figure 11 The erosion rate fell approximately linearly with increasing hardness if both it and hardness were plotted logarithmically against each other.

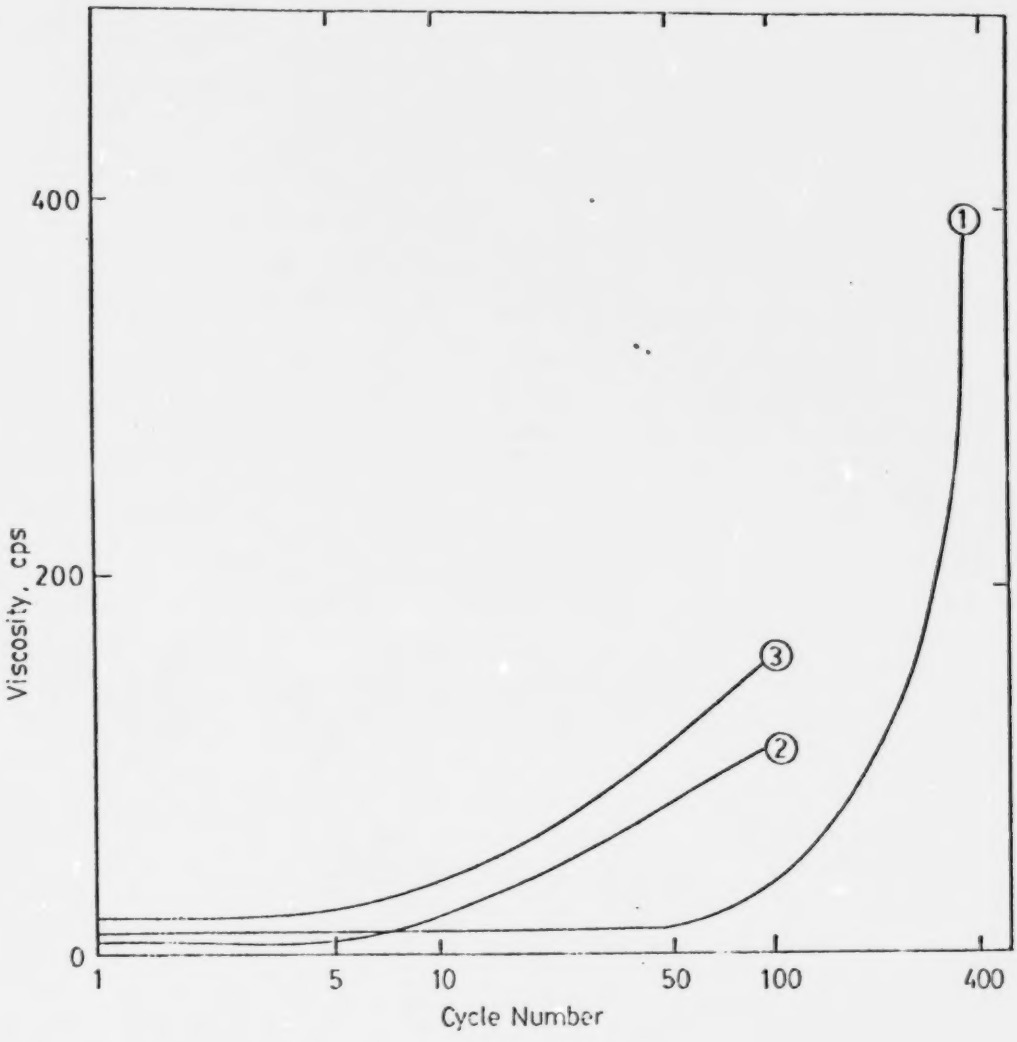

Figure 12 The effect of recycling upon viscosity was initially very slight but following repeated recycling then the viscosity increased quite rapidly and the abrasiveness of the slurry fell at the same time.

The pH of the recycled coal liquid mixtures also exhibited an initial period in which there was no change in pH after which the pH dropped. Figure 13 displays this behaviour for the three trials. The change in pH is due to the probable chemical reaction of the coal minerals, largely iron sulphide and to some extent chlorite, with the dissolved oxygen and water to form sulphate and chloride ions while removing hydroxyl ions as a result of the hydrolysis of ferric ions. These reactions, the end products of which are hydrated iron oxides and mineral acids, are almost certainly catalysed by bacteria and they lead to corrosive conditions which are discussed briefly in the appendix to this report.

If the changes with time of the pH and viscosity are now compared with the changes in erosivity of the coal liquid mixtures with respect to time, two conclusions can be drawn:

1. An increase in the viscosity of a slurry beyond 50 cps coincides with a decrease in the slurry's erosiveness. This was evident in all three trials.

2. The change in pH does not significantly alter the erosivity of the slurry.

Regarding this latter point, the slurry erosiveness is falling, in fact, as the slurry becomes more acidic and to common materials of construction, more corrosive. The "critical point" on the pH curve did not correspond with the "critical point" on the erosion curve as did that on the viscosity curve with its counterpart on the erosion curve. Corrosion must make some contribution to the weight loss as was observed in similar testing in which the relative velocity of the slurry to target was significantly lower (10) and has been observed in slurry transport tests at Saskatoon (11). However, it is felt that the target's weight losses due to the impingement of our slurry on the target are not significantly dependent upon corrosion for the spray velocity used here.

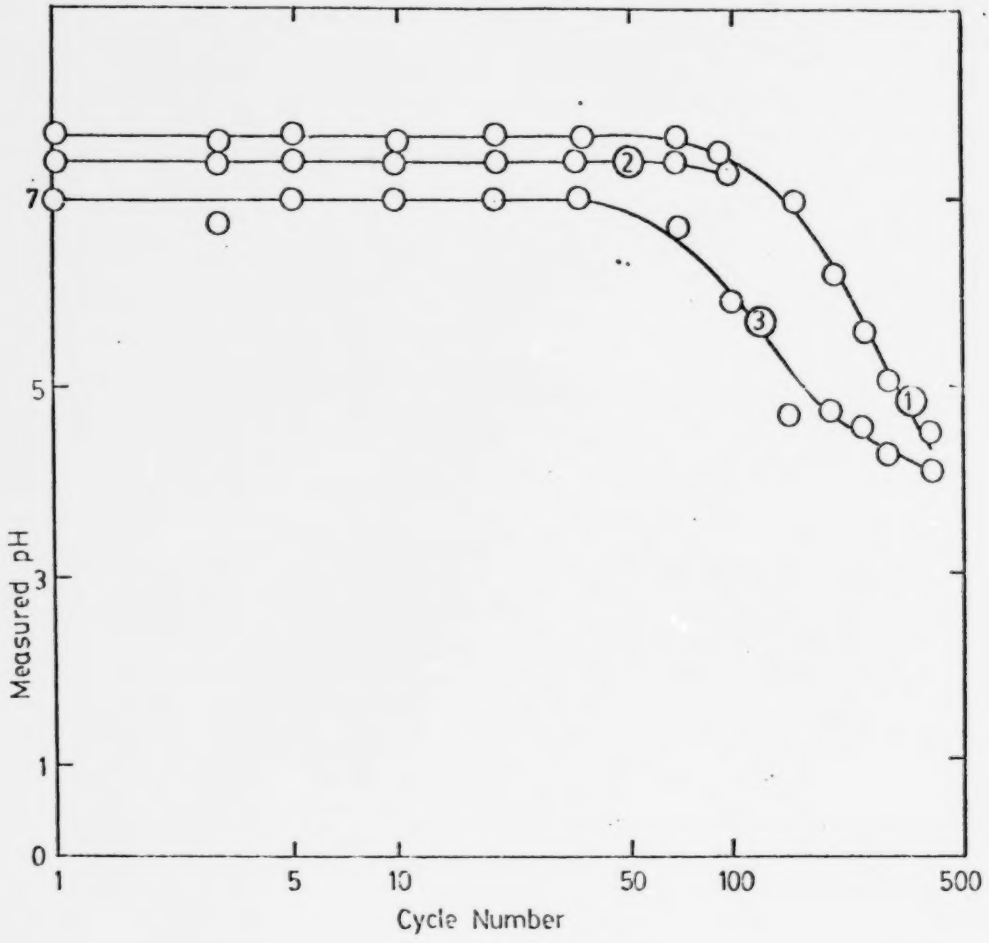

Figure 13 The pH of the slurry remained constant for 50 to 70 cycles and then fell quite rapidly, reaching a pH of 4 to 4.5 after 400 cycles. The commencement of the increasing acidity did not correspond with the rise in the viscosity or with the peak in the erosiveness curve.

4.3 Particle Size

Measurements of the coal's particle size following exposure for various lengths of time in the erosion trials indicates that the average grain size of the coal decreases with time. The coal grains are being abraded progressively from one slurry cycle to the next. Figure 14 illustrates this point while Tables 5, 6, and 7 contain all the particle size results.

If the particle size distribution results of the cycles which are nearest the peak of the abrasion curve in the Figure 5 are compared (70.36, 69.44, 68.66 % less than 325 mesh, 44 microns), they appear to be approximately equal. This conforms to the statement made earlier in section 3.2 that the viscosity of the CLM fuels increases as the coal is abraded from a certain point (for our tests approximately 69% less than 44 μm). Hence the slurry's abrasiveness started to fall as the viscosity reached 50 cps and this in turn occurred when the particle size fell to approximately 69% less than 44 μm.

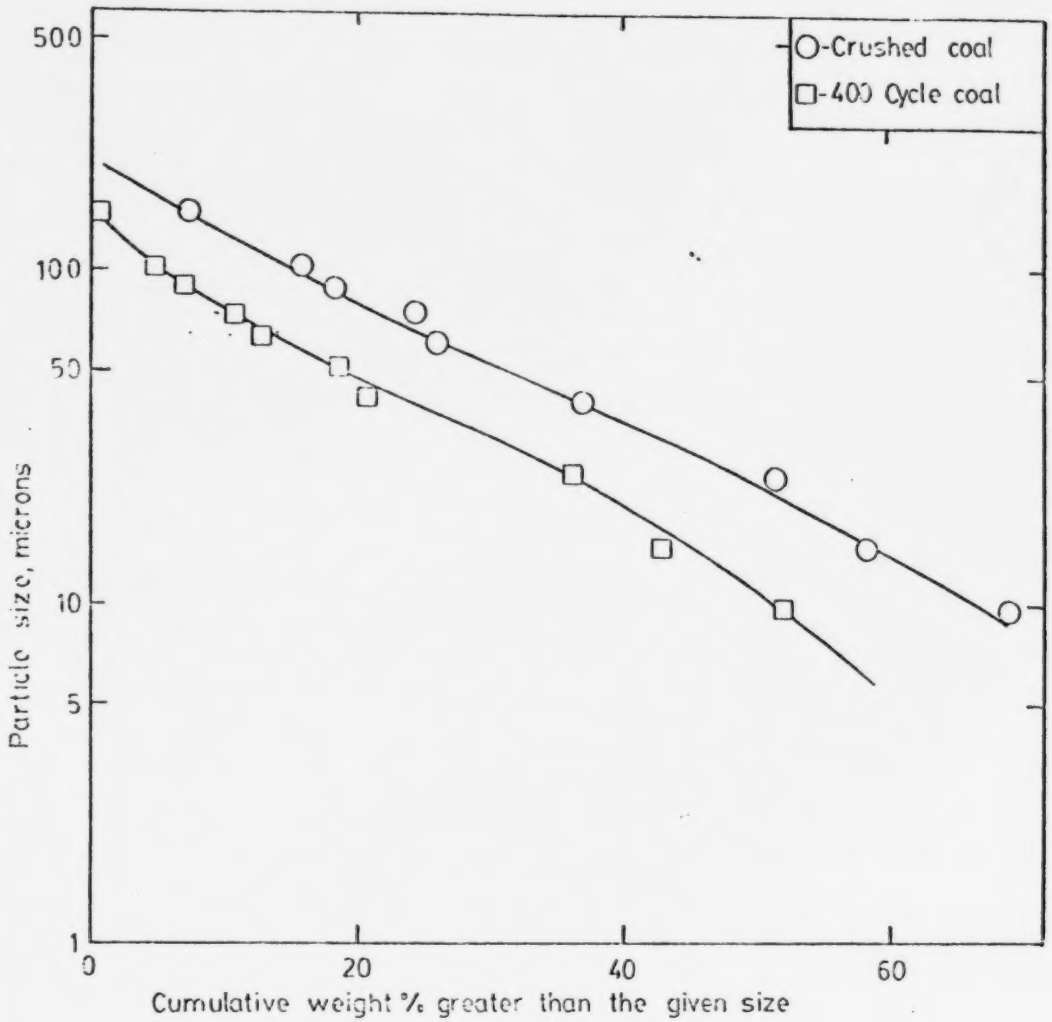

Figure 14 The coal particles became progressively finer as the slurry was recycled. The marked reduction in size here by about a factor of two, follows 400 cycles with impingement on a hardened 416 stainless steel target plate.

TABLE 5

Sieving Results of Trial 1

Cumulative Weight (%)

Mesh Size	(microns)	Cycle # 0	35	94	156	400
>100	(149)	6.7	5.67	4.26	2.77	0.6
>140	(105)	15.6	13.67	11.63	9.02	4.8
>170	(90)	18.1	16.60	14.04	11.73	6.8
>200	(75)	23.9	19.24	18.38	15.78	10.5
>230	(63)	25.7	23.97	20.93	18.78	12.6
>270	(53)	32.9	31.21	28.27	25.10	18.5
>325	(44)	36.4	32.67	29.64	26.61	20.3
<325	(44)	63.6	67.33	70.36	73.39	79.7

TABLE 6

Sieving Results of Trial 2

Cumulative Weight (%)

Mesh Size	(microns)	Cycle # 0	5	20	35	100
>100	(149)	5.9	5.50	5.54	4.81	3.8
>140	(105)	10.1	12.93	12.56	11.55	10.2
>170	(90)	16.7	15.87	15.62	14.54	13.0
>200	(75)	20.9	19.80	19.95	18.22	17.3
>230	(63)	23.0	22.87	22.61	20.72	19.4
>270	(53)	29.1	30.00	29.53	27.52	25.7
>325	(44)	31.5	31.20	30.56	29.07	27.1
<325	(44)	68.5	68.80	69.44	70.93	72.9

TABLE 7

Sieving Results of Trial 3

Cumulative Weight (%)

Mesh Size	(microns)	Cycle # 0	5	20	35	100
>100	(149)	6.93	6.21	5.58	4.81	0.68
>140	(105)	14.95	13.58	13.05	11.30	4.19
>170	(90)	17.82	17.01	15.77	14.27	5.71
>200	(75)	21.98	22.22	20.21	17.86	9.04
>230	(63)	23.84	24.76	23.44	20.89	10.83
>270	(53)	32.24	32.27	30.20	27.31	16.49
>325	(44)	33.61	34.14	31.34	28.21	17.56
<325	(44)	66.39	65.86	68.66	71.79	82.44

Tables 4, 5, and 6 display the coal particle size distribution for various recycling periods. The most significant fact obtained from these results is that the particle size distributions are similar at cycles 94, 20, and 20 for Trials 1, 2, and 3 respectively. These cycles are also important in that they are the points where the erosion peaks occurred in Figure 5 and when the viscosity was observed to exceed 50 cps in Figure 9. This allows the following conclusion: that a particle size decrease to a slurry with a particle size of approximately 69 percent less than 325 mesh (44 μm) results in an increase in viscosity above 50 cps and a decrease in erosivity of the slurry.

4.4 Mineralogy

Mineralogical examinations were performed either on bulk samples or on sink samples. A bulk sample would be a sample of the as-filtered coal which is representative of all of the sizes and constituents in the coal at a particular time. A sink sample would be that fraction which sinks in the specific gravity separations carried out at an S.G. of 2.4. The sink fraction is, of course, the dense material and is high in minerals which are free from adhering coal.

X-ray diffraction on that fraction of the coal sinking in a 2.4 S.G. fluid was employed to identify the mineral constituents, the results of which are contained in Table 8. This x-ray diffraction technique usefully gives the more abundant minerals present and hence those important to this study. Other minerals were identified using an oil immersion technique but due to their relatively small abundance, no further mention of these minerals will be made in this report. It is apparent from these results that over the course of the erosion trials, the relative abundance of several minerals has changed. The relative abundance of the minerals chlorite, magnetite, and siderite has decreased whereas the harder minerals (pyrite and quartz) have increased in relative abundance. However, pyrite is always the most abundant mineral in the sink fraction. The decrease in the relative abundance of the softer minerals may be because they are being leached into solution and mechanically degraded, so that they remain in suspension and were not recovered with the other solids. The pyrite and quartz grains appear to be progressively more liberated as the slurry was recycled. Particles of pyrite, for example, on association with coal matter would appear in the float fraction initially, but in the sink fraction following liberation. This would explain the appearance of an increase in pyrite particle size in the initial cycles of Table 10 (introduced later on in this paper).

An optical microscope (using reflected and transmitted light) was utilized to observe the mineral characteristics in a polished section (coal mounted in resin and polished using diamond abrasive) of sink

TABLE 8

X-RAY DIFFRACTION EXAMINATION OF THAT FRACTION SINKING IN A LIQUID OF 2.4 S.G.

Trial #	# of Previous Cycles	Order of Decreasing Relative Abundance
1	0	pyrite, with magnetite, siderite, and quartz, possible chlorite
1	35	pyrite, minor siderite, and magnetite
1	94	pyrite, siderite, traces of quartz, magnetite and chlorite
1	156	pyrite, siderite, minor quartz and magnetite, trace chlorite
1	400	pyrite, quartz, magnetite, siderite, trace chlorite
2	0	pyrite, magnetite, (probably some hematite), siderite, quartz, trace chlorite
2	5	pyrite, siderite, traces magnetite and chlorite
2	20	pyrite, siderite, trace magnetite
2	35	pyrite, siderite, possibly trace magnetite
2	100	pyrite, siderite, quartz, magnetite
3	0	pyrite, siderite, minor magnetite
3	5	pyrite, minor siderite and magnetite, traces of quartz and chlorite
3	20	pyrite, siderite, minor quartz, magnetite, chlorite
3	35	pyrite, siderite, possible trace magnetite
3	400	pyrite, minor siderite, traces quartz and magnetite

With the large error involved in making relative abundance measurements with x-ray diffraction results in mind, the quartz mineral appears to become more abundant with time, which may be explained by the grains becoming more liberated. The softer minerals (chlorite, magnetite, and siderite) have decreased in relative abundance, possibly due to leaching and particle size degradation.

samples obtained in the specific gravity separations. Mineral matter in the test samples was found mainly in very fine grains <20 microns with the exception of massive irregular pyrite grains which exceeded 100 μm.

Examination of bulk samples showed that most of the coal structure was destroyed in the crushing operation. Some of the coarser grains, however, still exhibited mineral matter filling fusinite cells, concentrating along bedding planes, filling microfractures and dispersed throughout vitrinite as spherical to subspherical blobs. The pyrite, in particular, was found mainly as liberated to semi-liberated irregular shaped grains and framboids that filled vitrinite and cells of fusinite. Some minor fracture fillings of the framboids were observed.

An image analyser or Quantimet was used for measuring the size and shape of pyrite grains in the heavy fractions, the results of which are listed in Tables 9, 10, 11, and 12.

The pyrite grains appearing in the sink fraction became coarser in the early cycles of exposure. At the same time the pyrite grains appeared to become more angular. The general trend throughout the erosion testing was a rounding and comminution of the pyrite grains and of the coal grains (see Figure 15). These statements appear to be conflicting ones but are reconciled if the larger pyrite particles which appeared in the sink fraction during the early cycles were ones which had previously been enveloped in, or at least attached to, coal matter. Hence the Quantimet was used in an attempt to measure the degree of liberation of the pyrite grains. The Quantimet could not distinguish, however, between the reflectiveness of the coal and that of the mounting medium: different mediums were used with little success. This determination was then performed using visual examination through a conventional microscope. The results generally indicated that the pyrite grains became more liberated with time (see Figures 16 and 17). Comparisons of pyrite freedom were made from the as-crushed coal and the recycled coal samples nearest the peak of the erosion tests. The results are displayed in Table 13. They indicate that a

significant amount of pyrite had been liberated or semiliberated by the time the peak in the curve of erosion versus slurry aging occurred.

Due to the problems with reflectiveness when using the Quantimet no work was performed to determine the shape, size, or changes in liberation of the quartz minerals in the coal. This is not considered of major importance since quartz was not as abundant as the pyrite and therefore not considered to be the major abrading mineral.

TABLE 9

THE SHAPE OF THE PYRITE GRAINS

Trial #	Number of Previous Cycles	Shape Range (%) < .01	.01 - .03	.03 - .06	> .06
1	1	28.58	34.64	29.30	7.48
1	35	11.16	50.20	26.07	12.57
1	94	20.22	48.01	28.35	3.42
1	156	26.05	43.81	22.83	7.31
1	400	0.83	15.40	59.12	24.66
2	0	11.07	49.63	34.01	5.29
2	5	7.31	51.66	27.66	13.37
2	20	16.70	43.15	31.55	8.61
2	35	22.24	46.90	24.95	5.91
2	100	9.33	34.59	47.53	8.56
3	0	17.67	32.90	37.55	11.87
3	5	19.52	41.12	28.31	11.05
3	20	15.41	42.66	30.64	11.29
3	35	29.54	33.52	28.96	7.98
3	400	7.84	26.49	52.75	12.93

These shape factors were calcuated from the surface area over the square of the perimeter using a Quantimet. Therefore in the columns headed "Shape Range" a value of less than 0.01 would indicate a long thin particle whereas a value greater than 0.06 is from a particle which is almost spherical.

The pyrite grains appear to become less round in the initial cycles due to pyrite grain liberation. This allows the pyrite grains that initially floated in the specific gravity separations (due to the adhering coal) to sink when this coal is liberated. This new influx of pyrite grains changes the existing shape patterns making the pyrite shape appear to become less round. This effect decreases with time as most of the pyrite grains become liberated and the pyrite grain shape (after 400 cycles) was observed to be significantly rounder.

TABLE 10

PYRITE PARTICLE SIZES IN THE SINK FRACTION FOR TRIAL 1

	0		35		94		156		400	
Particle Size (μm)	% at Indicated Size	Cumulative % Less Than Indicated Size	% At Indicated Size	Cumulative % Less Than Indicated Size	% At Indicated Size	Cumulative % Less Than Indicated Size	% At Indicated Size	Cumulative % Less Than Indicated Size	% At Indicated Size	Cumulative % Less Than Indicated Size
1.18	.00%	.00%	.00%	.00%	.01%	.01%	.01%	.01%	.00%	.00%
1.67	.01%	.02%	.00%	.01%	.02%	.03%	.02%	.03%	.04%	.05%
2.35	.04%	.06%	.04%	.04%	.11%	.14%	.09%	.12%	.25%	.30%
3.30	.18%	.24%	.28%	.33%	.22%	.36%	.15%	.26%	.85%	1.15%
4.70	1.46%	1.70%	1.17%	1.50%	.58%	.94%	.46%	.72%	3.06%	4.21%
6.60	3.48%	5.17%	2.49%	3.98%	1.57%	2.51%	1.25%	1.97%	5.61%	9.83%
9.40	5.72%	10.89%	3.33%	7.81%	3.87%	6.38%	3.20%	5.17%	9.91%	19.74%
13.20	8.45%	19.34%	7.29%	15.10%	5.49%	11.87%	4.98%	10.15%	16.16%	35.89%
18.60	9.33%	28.67%	5.90%	20.99%	8.26%	20.13%	6.33%	16.48%	29.78%	65.68%
26.30	13.87%	42.54%	7.86%	28.85%	9.65%	29.78%	10.79%	27.27%	19.72%	85.40%
37.10	18.49%	61.03%	12.31%	41.16%	15.60%	45.38%	19.11%	46.39%	4.03%	89.43%
52.40	22.95%	83.98%	17.75%	58.91%	12.71%	58.09%	20.80%	67.19%	0.00%	89.43%
74.00	9.09%	93.07%	33.87%	92.79%	18.04%	76.13%	8.63%	85.82%	10.57%	100.00%
104.50	6.93%	100.00%	7.21%	100.00%	23.87%	100.00%	9.22%	95.04%	0.00%	100.00%
147.40	0.00%	100.00%	0.00%	100.00%	0.00%	100.00%	4.96%	100.00%	0.00%	100.00%

Note here that initially we have 93 percent of the pyrite of a size less than 74 μm, after 94 cycles only 76 percent of the pyrite appearing in the sink fraciton has a size less than 74 μm, but this increases again hereafter so that after 400 cycles all the pyrite measured was less than 74 μm. Similar comments apply to the other runs. It appears that liberation, comminution, and rounding are progressing simultaneously.

TABLE 11

PYRITE PARTICLE SIZES IN THE SINK FRACTION FOR TRIAL 2

Number of Previous Cycles at Which the Size Analysis was Conducted

	0		5		20		35		100	
Particle Size (μm)	% at Indicated Size	Cumulative % Less Than Indicated Size	% At Indicated Size	Cumulative % Less Than Indicated Size	% At Indicated Size	Cumulative % Less Than Indicated Size	% At Indicated Size	Cumulative % Less Than Indicated Size	% At Indicated Size	Cumulative % Less Than Indicated Size
1.18	.00%	.00%	.00%	.00%	.00%	.00%	.00%	.00%	.01%	.01%
1.67	.01%	.01%	.01%	.01%	.01%	.01%	.02%	.02%	.02%	.03%
2.35	.05%	.07%	.08%	.09%	.03%	.03%	.04%	.06%	.16%	.19%
3.30	.21%	.28%	.32%	.41%	.15%	.18%	.26%	.31%	.73%	.92%
4.70	.81%	1.08%	1.04%	1.46%	.80%	.98%	1.15%	1.46%	2.41%	3.33%
6.60	1.62%	2.70%	2.55%	4.00%	1.43%	2.41%	2.41%	3.87%	4.55%	7.88%
9.40	3.05%	5.75%	5.86%	9.86%	2.76%	5.17%	3.31%	7.18%	9.11%	16.99%
13.20	4.70%	10.44%	7.02%	16.88%	4.66%	9.83%	4.72%	11.90%	12.11%	29.10%
18.60	7.56%	18.00%	14.94%	31.83%	8.27%	18.10%	5.77%	17.67%	15.04%	44.14%
26.30	10.63%	28.62%	20.93%	52.76%	8.47%	26.58%	13.39%	31.05%	18.43%	62.56%
37.10	19.34%	47.96%	10.76%	63.51%	12.44%	39.02%	14.91%	45.96%	25.96%	88.52%
52.40	37.54%	75.50%	15.55%	79.06%	15.98%	55.00%	25.98%	71.94%	11.48%	100.00%
74.00	20.87%	96.37%	6.67%	85.73%	12.87%	67.87%	11.50%	83.44%	0.00%	100.00%
104.50	3.63%	100.00%	0.00%	85.73%	21.03%	88.90%	16.56%	100.00%	0.00%	100.00%
147.40	0.00%	100.00%	14.27%	100.00%	11.10%	100.00%	0.00%	100.00%	0.00%	100.00%

TABLE 12

PYRITE PARTICLE SIZES IN THE SINK FRACTION FOR TRIAL 3

Number of Previous Cycles at Which the Size Analysis was Conducted

Particle Size (μm)	0		5		20		35		400	
	% at Indicated Size	Cumulative % Less Than Indicated Size	% At Indicated Size	Cumulative % Less Than Indicated Size	% At Indicated Size	Cumulative % Less Than Indicated Size	% At Indicated Size	Cumulative % Less Than Indicated Size	% At Indicated Size	Cumulative % Less Than Indicated Size
1.18	.00%	.00%	.00%	.00%	.00%	.00%	.00%	.00%	.00%	.00%
1.67	.01%	.01%	.00%	.01%	.01%	.01%	.00%	.01%	.00%	.01%
2.35	.02%	.03%	.02%	.03%	.02%	.03%	.03%	.04%	.02%	.02%
3.30	.14%	.18%	.13%	.16%	.30%	.33%	.08%	.12%	.08%	.10%
4.70	1.06%	1.24%	.81%	.96%	1.55%	1.89%	.58%	.70%	.32%	.42%
6.60	2.43:	3.67%	1.56%	2.52%	2.85%	4.73%	1.28%	1.99%	1.95%	2.37%
9.40	5.03%	8.69%	3.61%	6.14%	5.08%	9.82%	2.70%	4.68%	3.78%	6.15%
13.20	6.09%	14.79%	5.97%	12.11%	6.86%	16.68%	4.25%	8.93%	7.12%	13.27%
18.60	9.82%	24.61%	6.37%	18.48%	8.81%	25.49%	6.57%	15.50%	11.36%	24.63%
26.30	17.24%	41.85%	14.73%	33.21%	19.60%	45.09%	9.10%	24.61%	18.01%	42.63%
37.10	13.33%	55.19%	14.85%	48.06%	25.66%	70.75%	12.38%	36.98%	26.46%	69.09%
52.40	16.77%	71.95%	24.27%	72.33%	11.86%	82.61%	17.64%	54.63%	17.92%	87.01%
74.00	20.21%	92.16%	23.58%	95.91%	17.39%	100.00%	21.79%	76.42%	9.55%	96.56%
104.50	0.00%	92.16%	4.09%	100.00%	0.00%	100.00%	18.95%	95.37%	3.44%	100.00%
147.40	7.84%	100.00%	0.00%	100.00%	0.00%	100.00%	4.63%	100.00%	0.00%	100.00%

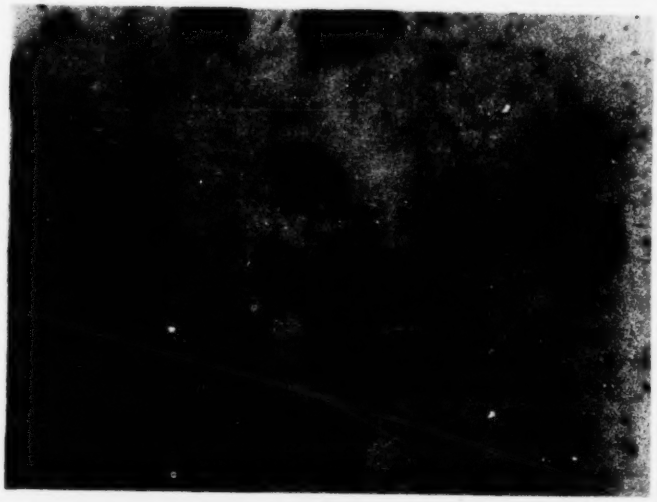

a. magnification x 64

b. magnification x 64

Figure 15

Coal grains which did not pass through the 100 mesh (149 μm) screen: (a) The sharp edged as-crushed (unstressed) coal grains; and (b) round coal grains of uniform size following 400 hours in the erosion test apparatus. These microphotographs were taken using reflected light on a conventional microscope of unpolished grains.

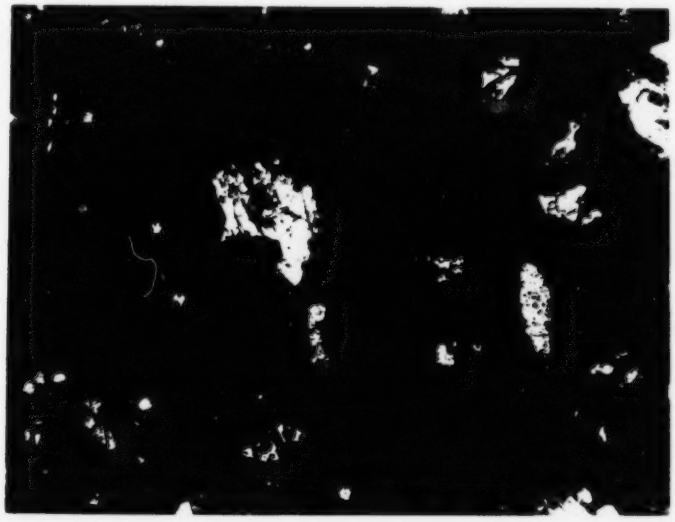

a. magnification x 131

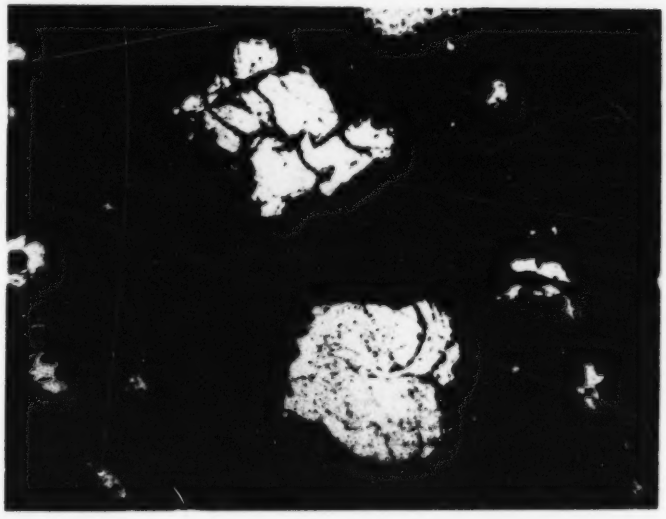

b. magnification x 260

Figure 16

Polished sections in which the mineral matter obtained from a specific gravity separation of an unstressed coal was mounted in an epoxy resin. The pyrite grains are observed to be white in colour and almost totally enveloped by coal: (a) The relative size and shape of the pyrite grains in the unstressed coal matter, and; (b) a higher magnification of (a) in which the small degree of liberation of the pyrite is clearly visible.

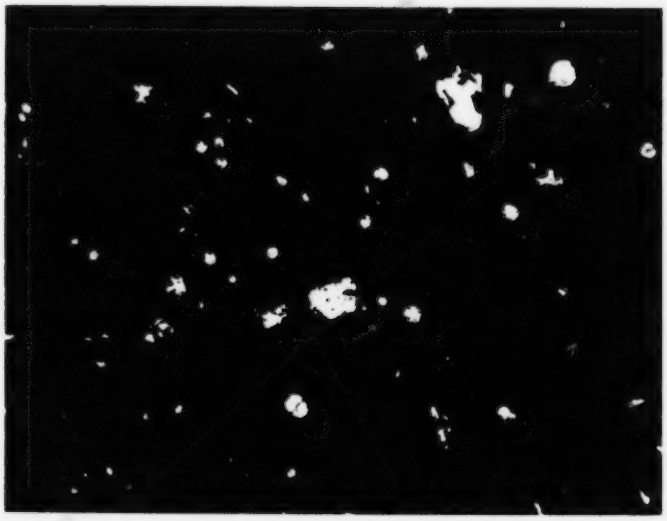

a. magnification x 131

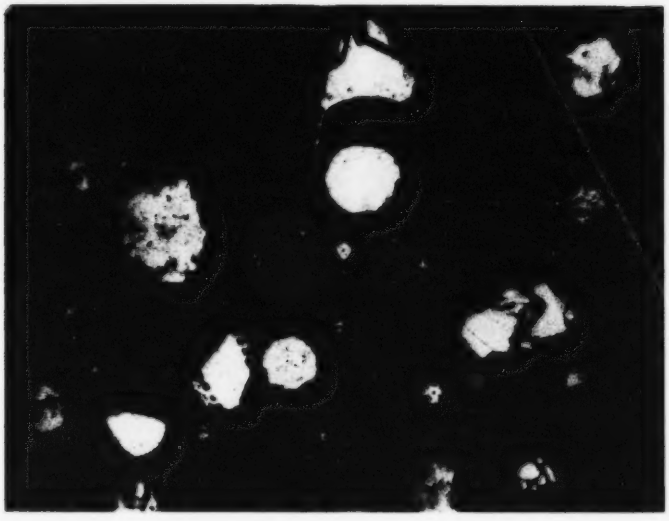

b. magnification x 260

Figure 17

Photomicrographs of polished sections of fully stressed (400 cycles) mineral matter mounted and prepared as in Figure 13. The pyrite attrition is observed in (a), while (b) illustrates the almost complete liberation of the pyrite grains.

TABLE 13

PERCENTAGE OF FREE PYRITE*

Run Number	Sample Number of Previous Cycles	Degree of Freedom (%) >50% Free	Degree of Freedom (%) <50% Free
1	0	14	86
1	96	36	64
2	0	47	53
2	20	49	51
3	0	20	80
3	20	26	74

* Measured using a conventional optical microscope at a magnification of 131 x for grains which were larger than 50 μm.

As shown above, the degree of liberation of the pyrite grains was observed to have increased by the time the peak in the erosion rate was observed in each trial.

5.0 DISCUSSION

5.1 The Erosive Peak: is this a slurry property or a hydrodynamic property?

The first question which should be answered is, was this peak, in the graph of erosion versus number of previous slurry cycles, a property of the slurry or a hydrodynamic property? The erosion trials with the various nozzles showed that the peak behaviour did not depend on the prior history of the nozzle. These results conflict with the earlier TUNS results where in similar trials peaking was probably not seen, hydrodynamic effects were important, and the prior history of the nozzle did have a bearing on the erosion of the target by the slurry. There are two differences between these trials and the TUNS trials and the first of these is quite definitely significant.

1. The nozzle used in the TUNS work was a drilled carbon steel nozzle which was seen to increase in its diameter from 3.175 mm to 3.373 mm in the course of a 500 minute trial. In contrast, the polished tungsten carbide wire drawing die used as a nozzle here did not increase its diameter measurably in the course of over 400 hours of operation. The severe nozzle erosion at TUNS during testing resulted in their erosion results having to be continuously adjusted due to the increased area exposed to the spray from a nozzle with a continuously growing orifice of changing shape.

2. The TUNS trials used a coal oil water mixture compared to coal water mixture trials here. There may be an effect on the erosion peak due to the different characteristics of a coal oil water mixture when compared to the CWM slurry used in these experiments. Having said all of this though, at least some of the data from the TUNS work (8) does fit a peaking curve similar to those curves obtained during the RPC trials.

5.2 The Cause of Peaking

Corrosion was not considered to be the cause of the erosion peaking, since the major pH change coincided with a negative, not a positive, slope of the erosion verses slurry recycling (slurry aging) curve. As the erosion rate was decreasing, the corrosion rate of aluminum was increasing (Appendix, part 3). The coal grain size was constantly decreasing as the slurry aged (Table 7). This can be expected to result in a continuous decrease in erosion rate. The reduction in slurry erosiveness following the peak in the erosion rate does coincide quite well with an increase in the viscosity of the mixture. This corresponds with the prediction of Al Taweel et al (8) that erosion by a solid/liquid mixture is inversely related to the viscosity of the liquid phase. Batra and Kenny (9) found that the CWM's viscosity depended inversely on the particle size and directly on the solids loading. The viscosity of the slurry does not appear to depend sensitively upon solids loading at a loading of 50 percent (12), which is the loading used in this test. The variation in the solids loading should not have had an effect on the overall erosion results and this was the observed pattern. The increase in the viscosity was, therefore, concluded to be a result of reduction in coal particle size. A primary effect of viscosity is to keep each particle in the fluid stream as the stream changes direction. The hydrodynamic forces on the particles tend to prevent the particles from striking the target and these hydrodynamic forces increase as the viscosity increases.

During the time in which the erosion was increasing the heavy minerals became liberated and semiliberated resulting in larger pyrite and probably also quartz grains being able to strike the target surfaces. It seems reasonable that the abrasion will increase as the number of hard large particles in the slurry increases. This has been suggested elsewhere (5) and it seems reasonable to suggest that the freeing of these grains would cause the slurry to become more erosive.

5.3 Significance of Peaking with Respect to Erosion Testing

Since the location and height of the erosion peak depends on both CLM properties and operational conditions, the exact peak position in any one trial cannot presently be predicted.

From the limited work performed here, the peak position would appear to move towards greater recycling times as the solids content is reduced and towards shorter times as the target plate's hardness is increased. This latter observation at least is reasonable: If the peaking behaviour is a function of particle liberation by abrasion, then the more efficiently the particles are abraded, by a hard target, the sooner we will reach and pass the peak.

If the trend of erosion peaking and the influence of viscosity upon this peaking is found in all possible mixtures, at high slurry flow rates, then two points could be made.

1. Erosion testing involving recycling could be conducted until an increase in viscosity is observed at which time the erosion test is concluded with that particular batch of slurry. The erosion rate over this period should have remained higher than the original slurry erosivity. This would result in weight losses that would be greater than those obtained when continuously using new slurry.

2. If the first type of testing is not satisfactory, then the erosion changes with respect to time must be determined for the slurry in question. This would allow average erosion rates to be calculated. These average erosion rates could then be applied to further erosion testing which would yield erosion test results that would best simulate service conditions.

5.4 Relative Erosion Resistance of the Four Target Materials

In Figure 11 is shown a plot which compares the erosion resistance of pure aluminum, hardened type 416 stainless steel, cemented tungsten carbide, and alumina with each material's hardness. It will be seen that the erosion resistance of alumina is significantly greater than that of the other materials and that erosion resistance increases with hardness according to a power law where the exponent is greater than unity. This observation conforms with earlier practical observations (1,2,3) with coal/oil mixtures.

A second observation with respect to hardness is that aluminum, hardened 416, and tungsten carbide all showed the same erosion behaviour. The erosion of both of the harder materials rose and fell in phase with the erosion of the soft aluminum. This would suggest that the erosion mechanism affecting all three is the same and that the erosion of one can be predicted from the erosion of another. Hence during component testing parts can be made up in a soft alloy which will erode rapidly, and this soft model can be used in erosion trials with a coal-water mixture to determine the best shape for least erosion; i.e., the hydrodynamic factors can be optimised and the design can then be manufactured in tungsten carbide with a reasonable assurance that the design will also be a hydrodynamically optimum one in that material. We cannot presently extend this prediction to alumina since not enough alumina was tested to determine whether or not it followed the same pattern as the softer materials did.

6.0 CONCLUSIONS

1. The erosivity of a 50 percent coal 50 percent water slurry (75 percent less than 200 mesh) is not a monotonic function of recycling but initially increases, peaks and then the erosivity falls.

2. Erosion testing using recycled slurry is complicated by the erosion peaking behaviour observed, but recycled slurry can be used to yield conservative results.

3. Erosion testing by recycling could be conducted until the viscosity is observed to increase rapidly. This would result in erosion, over that test period, that is greater than had new slurry been used for the same test period.

4. The cause of the initial increase in the observed erosion is thought to be in the liberation of pyrite and other hard mineral constituents from encircling softer materials.

5. The decrease in the slurry's erosiveness after the erosion peak coincided with a large increase in slurry viscosity which in turn was caused by the reduction in coal matter's particle size. This viscosity increase is believed to be responsible for the erosivity decline.

6. Solids loading and pH did not significantly affect the erosion results.

7. A significant increase in viscosity coincided with 69 percent of the particles passing through a 325 mesh screen.

8. The slurry particles became progressively smaller and quite clearly rounded as recycling proceeded.

9. Alumina supplied by the Atlantic Research Laboratory was quite clearly the most erosion resistant of the four materials employed. The other three in order of decreasing erosion resistance were cemented tungsten carbide, hardened type 416 martensitic stainless steel, and pure aluminum metal.

10. The peaking behaviour in the erosion versus recycling curves was observed for aluminum metal, type 416 steel and tungsten carbide. The peaks were all in phase during any particular trial.

7.0 REFERENCES

1. Thornley, J. C., "Nozzle Erosion During Slurry Firing, Chatham GS, 1978-1979"; RPC Report No. E/79/64; May 1979.

2. Whalen, P. J., Davies, F. W., Lee, L. K., and Mitchell, K. A., "A Study of Coal Agglomeration and Coal-in-oil Mixture Combustion in a Utility Boiler Period: June 1978 to July 1979"; prepared for the Federal Department of Energy, Mines and Resources; D.S.S. Contract No. 18SQ23440-7-4055-IV; September, 1979.

3. Whaley, H., and Whalen, P. J., "Burner Nozzle Wear During Coal-oil-mixture (COM) Combusion Trials in a Small Utility Boiler"; presented at Corrosion '81 International Corrosion Forum; Toronto; April, 1981.

4. Raask, E., "Erosion by Ash Particles in Coal-fired Boiler Plants"; V.G.B. Kraftwerkstechnin, 59(6), 1979, pp. 496-502.

5. Raask, E., "Input Erosion Wear Caused by Pulverized Coal and Ash," Proceedings - 5th International Conference on Erosion by Solid and Liquid Impact, 1979, pp. 41(1-7).

6. G. P. Tilly, Wear, 14 (1969) 63-79.

7. Meyers, Robert A., (1982), Coal Structure, Academic Press Inc., New York.

8. Al Taweel, A. M., Murphy, G., and Covill, I. D., "Erosion of Materials using Recirculated Coal-Liquid Mixtures"; Report prepared for Atlantic Research Laboratory, National Research Council of Canada; Contract No. 10SC.31028-1-2339; 1982.

9. Batra, S. K., Kenney, R. B., "Rheology and Pumping Characteristics of Coal-water Slurry Fuels Prepared in a Columbia Chase Integrator"; Fifth International Symposium on Coal Slurry Combustion and Technology; Tampa, p. 1119; 1983.

10. Hoey, G. R., and Bednar, J. S., "Erosion Corrosion of Selected Metals in Coal Washing Plant Environments"; Materials Performances, p. 9; April, 1983.

11. Shook, C. A., Haas, D. B., Husband, W. H. W., and Small, M., "Relative Wear Rate Determinations for Slurry Pipelines"; Journal of Pipelines, p. 273; 1981.

12. Al Taweel, A. M., Fadaly, O., Kwak, J., MacKay, G. D. M., McKee, W., "Rheological Properties of Coal/water and Coal/oil/water Mixtures"; Fourth International Symposium on Coal Slurry Combustion; Orlando; 1982.

APPENDIX 1

CORROSION OF METALS BY COAL-WATER MIXTURES

The work described in this appendix was not a necessary part of the contract between RPC and EMR (DSS) but corrosion is thought by RPC to be important and these few trials and observations were performed without affecting the cost of the work.

INTRODUCTION

Consideration of the breakdown of coal matter in a coal water slurry due to chemical and bacterial agents has led the authors of this report to become concerned about corrosion of metals by coal-water fuels. It is the concentration of possible oxidation products of coal that could cause drastic changes in the corrosion behaviour of the coal-water fuel.

These fears were realized after the first erosion trial was completed and a stainless steel (grade 304) tank in which the slurry had been stored was drained of slurry and quite severe pitting corrosion was revealed. Hoey and Bedmar (1) conducted erosion experiments and found that, at low velocities, corrosion resistance was more important than material hardness. Or in other works, that resistance to corrosion by coal-water slurries was more important than wear resistance at low velocities.

EXPERIMENTAL PROCEDURE

1. A brief corrosion analysis was performed on the storage tank corrosion to determine the type of corrosion and possible causes.

2. Several corrosion coupons were then prepared for exposure in the storage tank during the second and third erosion trials. Samples of carbon steel, galvanized carbon steel, and Grade 304 stainless steel were weighed and placed in the storage tank which contained freshly mixed coal-water slurry (50 percent, by weight, coal to water). Also samples of both the carbon steel and the stainless steel were autogenously TIG welded to provide them with heat-affected zones without the complications of a dissimilar weld deposit. Two specific corrosion situations were investigated: corrosion which occurs at the slurry-air (water line) interface and the corrosion which occurs at the bottom of the storage tank. In both cases the exposed samples were electrically isolated from each other and from the tank and other metallic components.

3. Aluminum target specimens were prepared to NACE Specification TM-01-69 and corrosion tested in agitated coal-water slurries which were either unaged (as-mixed) or aged to 300 cycles (recycled in the erosion test apparatus 300 times). This was carried out in order to examine the effects of the chemical changes in the aqueous phase upon its corrosiveness towards aluminum.

RESULTS

1. Examination of the Corrosion of a Stainless Steel, Grade 304, Storage Tank by Coal-Water Slurries.

Localized attack had occurred to several areas of the storage tank (see Figure A1). The pitting was generally associated with areas that had been welded and had progressed to a maximum pit depth of 0.48 mm.

One of the areas of pitting which was not associated with structural welding was cut out and prepared for metallographic examination. This pit had a maximum depth of 0.44 mm and is shown in Figure A2. No microstructural defects were observed as indicated by the normal austenitic grain structure illustrated in Figure A3.

2. Corrosion Testing With Ferrous Alloys

2.1 Corrosion of Various Ferrous Materials When Held at the Air Slurry Interface (Water Line)

The corrosion results of the water line experiments, which were conducted for 860 hours, are contained in Table A1. Both welded (heat-affected) corrosion coupons, carbon and stainless steel, experienced pitting along with general corrosion (see Figure A4). The maximum pit depth was 0.43 mm for the 304 stainless test coupons. The carbon steel corrosion coupons experienced the highest weight loss (6.1170 g for the unwelded coupon) with a general corrosion rate of 0.48 mmpy (calculated as per NACE Standard TM-01-69). The galvanized coupons had the next highest weight loss (5.46750 g) with almost complete loss of the zinc coating. The 304 stainless coupons (unwelded) exhibited the best resistance to general corrosion with a weight loss of 0.02895 grams.

TABLE A1

Water Line Corrosion of Various Materials
Due to Coal-water Fuels

Sample Type	Heat-Treatment	Measured Weight Loss (g)	Corrosion Rate (mmpy)	General Appearance
Stainless steel	welded	0.25270	__+	pitting in the heat-affected zone to a depth of 0.43 mm
(Grade 304)	unwelded	0.02895	__+	pitting at one corner of the coupon
Carbon Steel	welded	5.71230	__+	general corrosion with shallow pitting in heat-affected zone
	unwelded	5.14545	0.48	general corrosion
Galvanized steel	unwelded	5.46750	__++	general corrosion of carbon steel and the zinc coating was almost completely dissolved

\+ was not determined due to the pitting attack

++ could not be accurately determined due to the protective properties of the galvanized coating and unequal corrosion rates across the sample

None of the above materials was adequately resistant to corrosion by raw oxygenated and aged coal-water fuels suggesting further work is necessary.

2.2 Corrosion of Various Ferrous Materials when Placed at the Bottom of a Storage Tank During Erosion Testing

The corrosion results are displayed in Table A2. This corrosion test of carbon steel, stainless steel, and galvanized carbon steel was conducted for a period of 1340 hours. The welded carbon sample contained some shallow pitting in the HAZ, general corrosion, and had a much higher weight loss when compared to the unwelded carbon steel coupon (12.83410 to 6.1170 grams). The galvanized corrosion coupon exhibited a smaller weight loss of 3.3544 grams but the zinc coating had almost totally corroded away as in the water line tests. The stainless steel (Grade 304) samples exhibited the best corrosion resistance at 3.9×10^{-4} mmpy, but exhibited pitting attack in the heat-affected zone of the welded coupon (see Figure A5). The maximum pit depth in the stainless steel was 0.36 mm.

TABLE A2

Corrosion of Various Materials
Placed at the Bottom of a
Coal-water Fuel Storage Tank

Sample Type	Heat-Treatment	Measured Weight Loss (g)	Corrosion Rate (mmpy)	General Appearance
Stainless steel	welded	0.05930	__+	pitting in the heat-affected zone to a maximum depth of 0.36 mm
(Grade 304)	unwelded	0.00770	3.9×10^{-4}	no evidence of corrosion was observed
Carbon Steel	welded	12.83410	__+	general corrosion and shallow pitting in the heat-affected zone
	unwelded	6.1170	0.33	general corrosion

Sample Type	Heat-Treatment	Measured Weight Loss (g)	Corrosion Rate (mmpy)	General Appearance
Galvanized steel	unwelded	3.3544	++	zinc coating was almost completely dissolved and the general corrosion of the carbon steel had occurred

+ was not determined due to the pitting attack

++ corrosion rate could not be calculated due to the effects of the zinc coating.

In this trial unwelded type 304 stainless steel did perform adequately but none of the other tested materials including welded type 304 was adequately resistant to corrosion by coal-water fuels. Further work is again suggested to determine the cause of the attack and possible procedures for preventing this corrosion.

3. Corrosion Testing of Some Aluminum Target Specimens

This test was carried out as per NACE Specification TM-01-69 for a period of 74 hours. The average weight loss of the three aluminum samples in the unaged slurry (as-mixed) was 2.3 milligrams as opposed to 6.6 milligrams for the slurry which was aged to 300 cycles.

DISCUSSION

The pitting of carbon and stainless steel (Grade 304) was almost completely restricted to the heat-affected zones of the welds in the storage tank and corrosion test coupons. These areas are known to be particularly susceptible to corrosion due to carbide growth. However, further work is necessary to determine what caused the corrosion before soundly based suggestions could be made as to how to combat the coal-water fuel's corrosive nature.

The increase in the slurry's corrosiveness with recycling indicates that the coal matter breakdown has a significant effect on the corrosiveness of a coal-water fuel. This should have been expected, since the breakdown of coal matter results in increase in dissolved mineral matter and formation of acids.

Important factors in determining the corrosiveness of the coal-water mixture are inorganic and physical factors such as the degree of oxygenation, the time of exposure to oxygenation, the coal's minerals (particulary the presence or absence of alkaline minerals), and the buffering effects of additivies. Organic factors may, however, be of supreme importance. In particular one must consider the presence or absence of aerophilic sulphur (and sulphide) oxidizing bacteria and also of aerophobic sulphate reducing bacteria which can promote pitting of both carbon and stainless steels (2).

CONCLUSIONS

1. Corrosion by coal-water fuels is a significant problem when recycling fuel mixtures.

2. Corrosion by a recycled fuel preferentially attacks heat-affected zones of carbon and stainless steel (Grade 304) welds.

3. Breakdown of the coal and coal mineral matter does result in an increased corrosion rate.

REFERENCES

1. Hoey, G. R. and Bedmar, J. S., "Erosion Corrosion of Selected Metals in Coal Washing Plant Environments," Materials Performance, Vol. 22, April 1983, p. 9.

2. Microbial Aspects of Metallurgy, ed. J. D. A. Miller, Med. and Tech. Press, Aylesbury, 1971.

Figure A1

The localized corrosion of the 1140 litre coal-water fuel storage tank. The pitting attack was mainly associated with heat-affected zones of the tank's welds.

Figure A2

Magnification x 5

A corroded area of the stainless steel storage tank. Note how the area is growing in size by the initiation and growth of pitting around its perimeter.

Figure A3

Magnification x 131

Microphotograph of one of the corrosion pits of the stainless steel storage tank. The microstructure is that of a normal cold-rolled austenitic grade 304 stainless steel. No microstructural defects were present that would explain why the pit developed in this area. It is possible then that some setting of the coal had occurred in this area and an oxygen concentration cell was formed. In addition, bacterial agents might have been influential in initiating and deepening the pits.

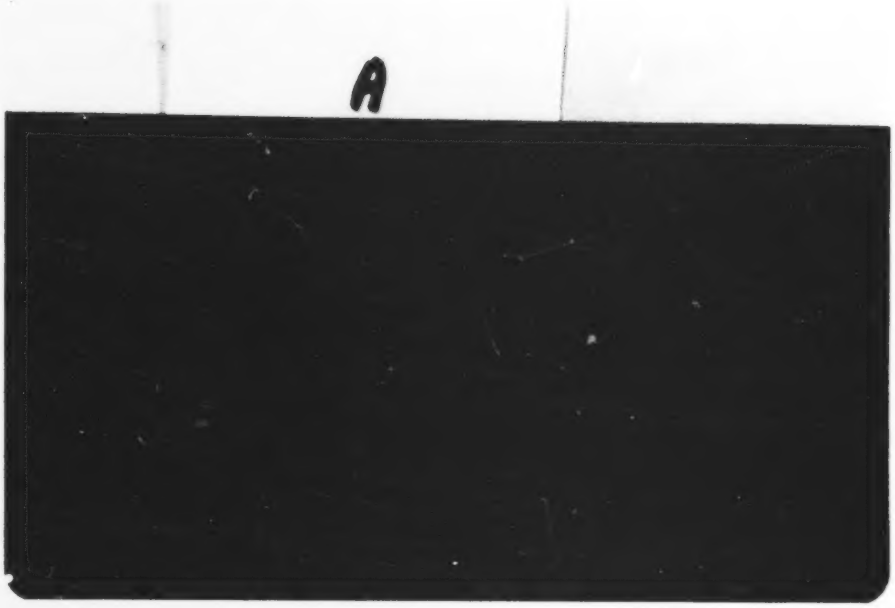

Figure A4

General and localized corrosion of a carbon steel test coupon which contains a heat-affected area. The heat-affected area was produced by melting the plate with an arc from a nonconsumable welding electrode.

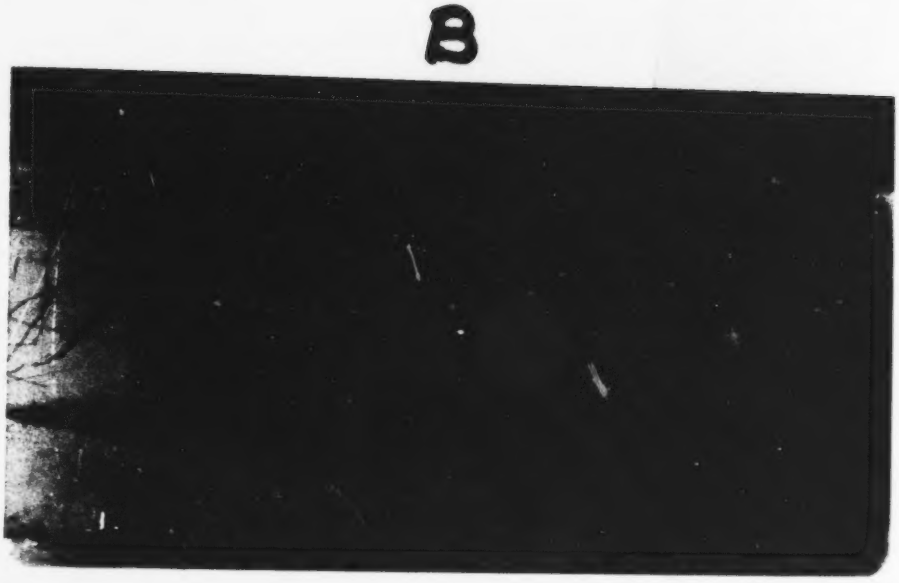

Figure A5

The autogenously welded stainless steel (grade 304) corrosion test coupon just after it had been taken from the storage tank. Note how the pitting is concentrated along the weld's heat-affected area. This sample is the one which was exposed at the slurry water line.

POOR

QUALITY

ORIGINAL